FACULTY OF SCIENCE AND TECHNOLOGY

MASTER THESIS

Study programme / specialisation: Production and processing

The spring semester, 2022

Open / Confidential

Author: Maria Laugtug Jacobsen

(signature author)

Course coordinator: Øystein Arild

Supervisor(s): Rune Wiggo Time, Andrianifaliana Herimonja Rabeniafimanantsoa

Thesis title: Experimental study of CO_2 absorbtion and desorption in WBS

Credits (ECTS): 30

Keywords: CCS, mass transfer, pressure decay,

Pages: ……57……

+ appendix….10……

Stavanger...29/06…..
date/year

University of Stavanger

Faculty of Science and Technology

EXPERIMENTAL INVESTIGATION OF ABSORPTION OF CO_2 IN WATERBASED SOLUTIONS.

Supervisor of Thesis: Rune Wiggo Time, Andrianifaliana Herimonja Rabenjafimanantsoa .

By

Maria Laugtug Jacobsen

A Thesis Submitted to
the Faculty of Science and Technology
in Partial Fulfillment of the Requirements for the Degree of
Masters of Science

15th of June, 2022

ABSTRACT

An investigation of Carbon dioxide (CO_2) absorption and desorption is carried out to understand the diffusion and flow mechanism of a pressurized CO_2 gas cap in an water-based solution (WBS) and to accurately quantify the CO_2 absorbed by the system. This is particularly of interest to further understand the behaviour of CO_2 when injecting it into an aquifer reservoir for permanent storage, however it proves to be useful knowledge for several applications for the carbon capture and storage process cycle. A series of pressure decay experiments were carried out in a non-invasive PVT cell able to withstand pressures up to 7 bar. The cell is cast in an epoxy block to avoid visual phenomenon's, and is transparent to allow for the flow mechanisms to be apparent. To further highlight the flow mechanisms pH indicator was added to the alkaline solution. The experimental data was accompanied by a video recording for each experiment to understand the relation between the mass transfer patterns, pressure and saturation of the system.

The experimental data pressures were analysed using a simple pressure boundary model, for the diffusion coefficient and final saturation pressures to be calculated. Once saturation pressure was reached the WBS was flashed to atmospheric pressure to accurately quantify the CO_2 absorbed. This allowed for a mass balance of the CO_2 to be carried out to accurately quantify the moles absorbed by the WBS at the different pressures.

ACKNOWLEDGMENTS

Firstly I would like to acknowledge my sincere appreciation for Professor Rune Wiggo Time and Senior Engineer Andrianifaliana Herimonja Rabenjafimanantsoa who has provided me with excellent support and guidance throughout the laboratory work and the writing of the thesis.

Besides my supervisors to express my thanks to my partner, friends, family and colleagues at PXO for supporting me throughout the time consuming process a laboratory based thesis can be.

OBJECTIVES

The focus of the thesis carried out was to further understand the absorption and desorption mechanisms of carbon dioxide in a water-based solution upon depressurisation through flash distillation. The results obtained from this study can be applied to several aspects of the carbon capture and storage sequence, and is particularly relevant for the storage of CO_2 in deep aquifer formations. When supercritical CO_2 is injected into the reservoir a pressure increase will occur and a pressurized CO_2 plume will, due to buoyancy, form under the cap rock. Due to the pressure differences mass transfer will occur until the system reaches equilibrium.

Instability around the gas-liquid interface occurs due to the formation of carbonic acid, which has a higher density than water, causing convection to be the dominant intermediate mass transfer mechanism. This is positive when applied to storage as the CO_2 sinks deeper in the reservoir. However there is always a risk of leakage due to faults in the formations causing a pressure release, initiating rapid desorption of CO_2 . Utilising a flash distillation setup where the WBS containing CO_2 goes from the saturated pressure to atmospheric pressure it is possible to accurately quantify the amount absorbed and desorbed.

To visualize the fluid dynamics the alkaline water employed a pH indicator solution to further visualise and understanding of the mass transfer mechanisms. A range experiments were carried out to investigate how the magnitude and pressure of the CO_2 injected and the salinity of the WBS has on the systems behaviour.

TABLE OF CONTENTS

List of Figures

List of Tables

Nomenclature

Abbreviations

CCT	Carbon capture technology
WBS	Water based solutions
SMR	Steam methane reforming
CCS	Carbon capture and storage
NG	Natural gas
NCS	Norwegian continential shelf
IR	Infrared radiation
MEA	Monoethanolamine
BTB	Bromothymol blue
PVT	Pressure-Tempreature-Volume

Chemical compounds

$NaOH$	
CO_2	Carbon dioxide
H_2O	Water
CO_3^{-2}	Carbonate ion
H^2	Hydrogen
H_2CO_3	Carbonic acid
HCO_3^-	Bicarbonate ion
N_2	Nitrogen
Na_2CO_3	Sodium carbonate
$NaCl$	Sodium chloride
$NaOH$	Sodium hydroxide
O_2	Oxygen
OH^-	Hydroxide ion

Symbols

P_{sat}	Saturated pressure
P_i	Initial pressure
ρ	Density
α	Thermal expansion coefficient $[K^{-1}$
β	Volumetric expansion coefficient $[m^3/mol]$
X	Storage efficiency factor
δ	Atomic charge [C]

μ	Dynamic viscosity
γ	Specific gravity
κ	Wave number $[m^-1]$
v	Kinematic viscosity $[m^2/s]$
ρ	Density $[kg/m^2]$
τ	Positive time constant
$\vec{J}$	Diffusion flux
$\vec{r}$	Position vector
A	Area $[m^2]$
At	Atwood number
c	Concentration $[mol/m^3]$
D	Diffusion coefficient $[m^2/s]$
D_T	Thermal diffusitivity $[m^2/s]$
g	gravitational acceleration $[m/s^2]$
h	Height of gas $[m]$
K_H	Henry's law constant $[m^3Pa/mol]$
L	Liquid height $[m]$
M	Molecular mass $[kg/mol]$
n	Number of moles $[mol]$
P	Gas pressure $[bar]$
R	Universal gas constant [J/molK]
r	Radius $[m]$
Ra	Rayleigh number
T	Temperature $[^\circ C]$
t	Time $[s]$
V	Volume $[m^3]$
v	Velocity $[m/s]$
V_{gp}	Volume gas $[m^3]$
V_l	Volume liquid $[m]$
Z	Gas compressibility factor for $CO_2[m]$
SF	Scale up factor

Chapter 1

Introduction

The scientific community has over the past 150 years observed a significant and consistent increase of greenhouse gas (GHG) emissions. When analysing the timeline of industrialisation and increase of population and comparing this with data concerning GHG's, it is clear that anthropogenic activities are the cause of the global temperature increase. There are many concerns linked to the climate scenario currently unfolding, the most significant ones being rise in sea level, decrease in biodiversity and extreme weather. Collective initiatives have been established across nations to mitigate permanent destruction of habitat. The most significant global initiative to date is the Paris Agreement by The United Nations Framework Conventions on Climate Change (UNFCCC). The main objective of this agreement is to keep the global average temperature to no more than 2 $^{\circ}C$ higher than pre-industrial levels, mainly through GHG emissions(1). Despite the atmosphere consisting of a range of gases, only some are in the category GHG. Carbon dioxide (CO_2) is considered to be the most damaging GHG due to the magnitude it is being emitted today. The chemical properties that make CO_2 a problematic gas to the temperature of the atmosphere will be further elaborated on in chapter 1.2.1 CO_2 structure and properties

To achieve the reduction in GHG emissions all countries who have signed the Paris Agreement are required to cut their carbon dioxide by 7.6 % every year for the next decade, which equates to 6 billion tonnes globally every year. It is clear this is a significant reduction that require technological mitigation strategies. Renewable energies are a great method of cutting emissions from the power and industrial sector, but to maintain the lifestyle we know today, where; travel, exotic foods and spices, animal products and material goods are luxuries many enjoy as a part of everyday life, further mitigation measures are required. There is simply currently not enough renewable energy to cover the global demand, so other methods of emission mitigation initiatives must be implemented(2).

As Norway has had hydroelectricity as its main form of energy source for the last century, it has a low rate of CO_2 emission as a nation in comparison to other country. It can therefore seem strange that CCS is an area of great interest for both the government and industry. There is no immediate need to implement the technology, unlike countries where majority of the power grid and industry is powered by coal. The reasoning behind the interest can be divided into three main drivers(3).

The first societal driver dates back the furthest, and is the high level of ambition in environmental protection amongst the people and politicians in Norway, and the large presence of environmental activist organisations. It has been an area of focus for the energy industry since the late 1980's as a result of the sudden growth of the oil and gas industry and the emissions from these activities.

Secondly, Norway has a wealth of knowledge and project opportunities through well-established oil and

gas companies and educational facilities proving to be useful and transferrable for CCS. The pioneering CCS storage project Sleipner, carried out by Equinor (former Statoil) is a great example of the political encouragement and the oil and gas industry in Norway. At this facility the CO_2 is removed from the natural gas (NG) and injected back into the reservoir. This was motivated by a CO_2 tax applied to the oil and gas industry, which at the time was unique to Norway.

The last driving force for CCS builds on the global political climate and the energy shift towards more environmental friendly energy forms. Norway is currently one of the largest exporters of NG to Europe, with pipeline systems from Norwegian gas production fields and processing facilities to gas receiving facilities in Scotland, England, Germany and France. Converting this gas to blue hydrogen through steam methane reforming (SMR) followed by CCS is an opportunity for Norway to maintain their key position as energy suppliers when NG is an unwanted product due to its emission upon combustion. The infrastructure laid in place for NG would need modification due to the different thermodynamic properties of the hydrogen molecule, however it is still an opportunity to utilise the existing infrastructure. The switch from NG to hydrogen as an electricity source is already apparent through the current development of hydrogen turbines carried out by all the major turbine manufacturers such as Mitsubishi, GE and Linde.

As mentioned, we are globally moving towards more decarbonizing the energy and industrial sector. There has been a great focus on battery technologies which has been a great success for light transportation vehicles. However, it is unfeasible to implement this technology for heavy duty transport, such as large cargo ships and planes. This is due to the heavy weight of the battery as well as the energy demand being too high compared to the capacity of the battery itself. Hydrogen is a fuel that has already proven useful for this application as it is the fuel of choice for space travel (4). It is very energy dense and has no emissions upon combustion. In Norway there are several examples of ferries being built with hybrid solutions, utilising both battery technology and the hydro power in Norway, while using hydrogen to support the battery with electricity through a hydrogen fuel cell when the battery is not sufficient. This is indication of a growing demand of hydrogen in Norway. It is not feasible for 'green hydrogen', hydrogen produced through electrolysis from 'leftover' electricity, to be the sole production path as it does not cover the current, let alone growing energy demand as predicted. In order to produce hydrogen sustainably at magnitudes impacting the energy sector, decarbonisation of the SMR process is required.

In 2015 the full scale CCS project Longship was initiated by the Norwegian government to be carried out by Gassnova, a research institute dedicated to CCS, in cooperation with industry partners. The objective is to prove the viability of CCS as an industry opportunity for Norway(5).
CO_2 is captured from a cement production facility and a waste incineration facility in Eastern Norway and transported by ship to the CO_2 receiving terminal in Øygarden in Western Norway. From there the CO_2 is transported through pipeline to Oseberg A platform in the north sea. The CO_2 is injected at a depth of 2500 meters below the seabed into an aquifer. The realisation of this project, scheduled for 2024, will be a global statement proving Norway to be an industry leader within the field. However, it is estimated that up to 10 $GtCO_2$ will need to be removed annually from the atmosphere. For storage of this magnitude to be possible storage cannot be restricted to depleted oil reservoirs and the behaviour of CO_2 in different conditions need to be researched extensively to realise maximum storage capacity.

This chapter has highlighted the motivation behind further development of CCS on a global scale and locally in Norway. Understanding the behaviour of CO_2 upon transportation, injection and storage is particularly important for Norway as it is a gateway to maintaining the position as a key energy

supplier in Europe when Natural Gas (NG) is an undesirable product.

1.1 Overview of the Thesis

The physical properties of CO_2 and an overview of the CCS chain will be presented in Chapter 1.2. It contains an overview of the main processes with emphasis on technologies appropriate for Norway and the Norwegian continental shelf (NCS). This will be followed by a literature review of relevant studies that have been carried out where the findings can be employed for further development of the experiment and result analysis.

Chapter 1.4 connects the physical properties of CO_2 and the CO_2 storage conditions to mass transfer mechanisms. Thermodynamic theory that applies to the conditions is used to develop an analytical model used for comparison with the experimental results.

Chapter 2 gives a detailed description of the different aspects of the experimental setup procedures and is followed by Chapter 3 where the results from said experiments are presented. This chapter also contains an in-depth discussion of the validity and application of the results. Chapter 4 consists of the conclusion, summarising the main observations and findings. Lastly, chapter 5 discusses further work that can be done to elaborate and further justify the findings

1.2 Carbon Capture and Storage

1.2.1 CO_2 structure and properties

The levels of CO_2 in the atmosphere was recorded to be 423 ppm in 2020 (6). This is a low concentration when compared to other gases present in the atmosphere, such as nitrogen, oxygen and argon. Despite this, CO_2 is the gas causing the greatest concern in regards to the climate from both the public and scientific community. The reason for the concern is the complex molecular structure of CO_2 , causing it to be considered a greenhouse gas. The molecular structure enables it to absorb infrared radiation (IR) and later releasing it in all directions, which leads to some of it effectively being trapped in the atmosphere. As a result, heat from the sunlight will remain causing global warming (7).

For the sake of relevance, we only outline the properties of CO_2 . To be considered a greenhouse gas, a molecule needs to undergo quantum transition. Quantum transition is linked to vibrations between the bonds between the atoms. A bond dipole represents the charge separation in the bond. The bond dipoles can be quantified with a set of vectors. Summing these vectors will give the molecular dipole movement. In its ground state CO_2 does not have any dipole movement due to the bond dipoles cancelling.
CO_2 is able to absorb radiation due to undergoing a quantum transition by movements in its nuclei. This occurs due to vibration of the molecules as CO_2 has more than one atom. However, if the molecule absorbs energy, in this case from IR, it goes from the ground state to electronic excited state. There are three different vibrational excited states displayed in the figure below. The linear and non-polar nature of the CO_2 molecule only allows for asymmetric stretch and bending mode, displayed in figure 1.1, to result in a change in the dipole movement. This proves on a molecular level why CO_2 has the ability to cause global warming and highlights the importance to keep the levels of CO_2 in the atmosphere stable.

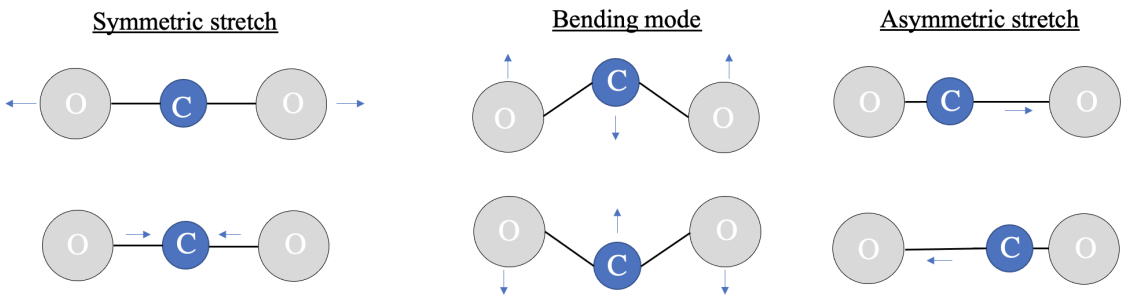

Figure 1.1: Dipole movement CO_2

1.2.2 Capturing Technology

Although the commercialisation of CCS has yet to become a success, there are already a range of accessible technologies that can be applied, and are established and commonly used in industry today. Most are usually employed as a method of purification for oil and gas processing to increase the quality, therefore the price of the product (8). When an industrial facility has removed the carbon dioxide, it is typically released back into the atmosphere as the price of further processing and utilisation or storage is higher than the associated carbon tax upon release.

CO_2 capture technologies can be split into three main categories for sake of simplicity; pre-combustion, post combustion and oxyfuel combustion. A simplified process flow diagram is displayed in figure 1.2 to outline the different processing paths.

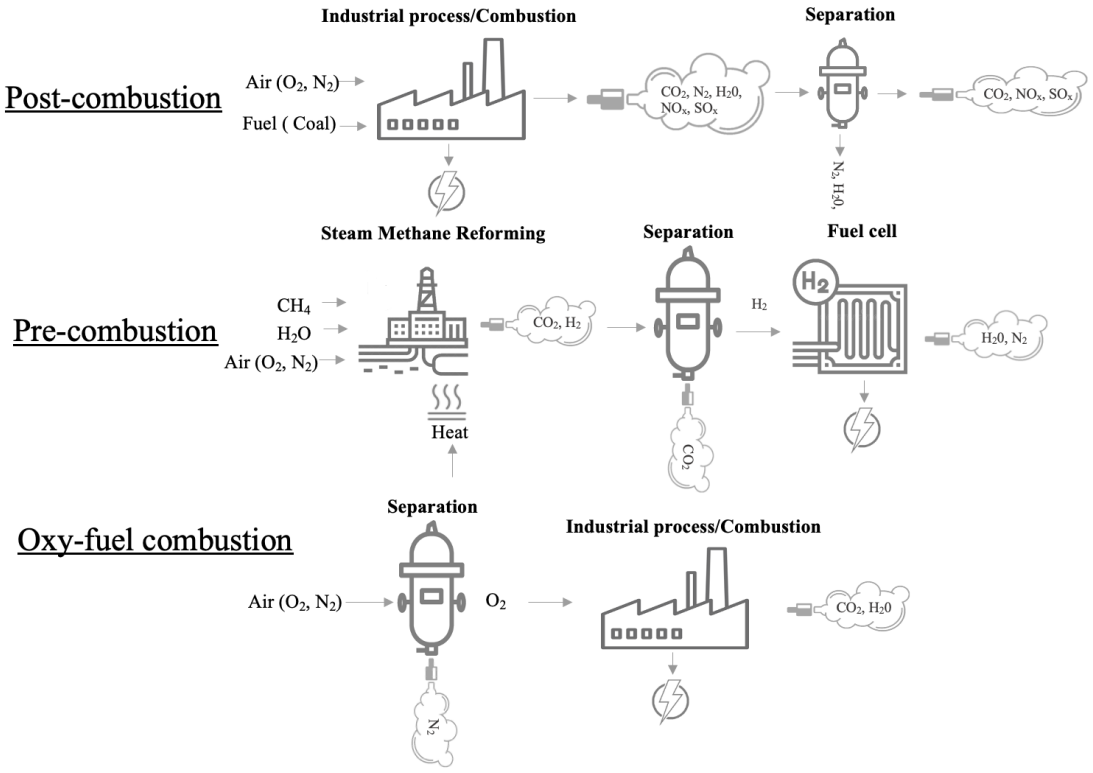

Figure 1.2: Carbon Capture Technology paths

Post-combustion CO_2 captures the emissions from combustion flue gases. Power plants, coal fired plants

in particular, accounts for 25% of the global carbon emissions. The post-combustion technology allows for the CO_2 to be captured from flue gas. Some alternative applications for this carbon capture technology (CCT) are the steel and concrete production industry. The flue gas typically has a composition of 8-14% CO_2 . The flue gas also contain other contaminants such as Sulfur- and nitrogen oxides and particulate matter which requires to be removed to satisfy the relevant control measures requirements in the relevant region. The most efficient separation method for CO_2 and flue gas is through chemisorption by monoethanolamine (MEA). The amine absorption process will remove between 85-90 % of the CO_2 in the flue gas. The following step consist of heating the CO_2 rich amine solution to release the CO_2 in a stripping unit. The CO_2 is then compressed as preparation for transportation, and the amine solution is recycled back into the absorption unit. The benefit of this technology is that it can be installed around a pre-existing industrial facility, allowing production out the expected lifetime while significantly reducing emissions. This is a more sustainable option opposed to abandoning or demolishing functional facilities, as the construction of a plant can be have larger emissions associated compared to the emissions from the running facility. The low concentration of CO_2 in the flue gas is the main limitation of this CCT. The complexity and energy required to separate pollutants from air are inversely related to the concentration of the pollutant in the flue gas.

In pre-combustion CCT the gas undergoes SMR producing primarily CO_2 and H_2, and some carbon monoxide due to incomplete combustion. The H_2 is separated from the CO_2 and can be utilised as a fuel with the combustion product being H_2O. The pre-combustion CCT is uses pressure swing absorption followed by gas-stripping. The separation step is complex due to the chemical properties of the absorbents used and results in an energy intensive process.

While it has proven to be a technology that mitigates pollution effectively, the pre-combustion capture plant has a higher capital cost and lower overall performance. The different applications for pre- and post-combustion CCT means plant efficiency of these processing pathways is not a fair comparison. It would be more suitable to compare pre-combustion CCT against other hydrogen-production pathways. Hydrogen production through electrolysis, also referred to as 'Green Hydrogen', is the competing alternative production path today. Though it is a great way to utilise excess electricity, it has some limitations that restricts the scale up potential. The first is that the it produces energy units of hydrogen at a small rate compared to the energy units of electricity put into the system. The second limitation is access to renewable electricity of large quantities. This highlights the first point regarding the large energy requirement for producing one unit of hydrogen. This has been especially highlighted in the past year where there has been an energy crisis in Europe, where there has been a higher electricity demand compared to previous years, and is not a viable option for production on a large enough scale to be an alternative to hydrocarbons. Per unit of hydrogen produced it is significantly less energy intensive to use SMR followed by CCS, often referred to as blue hydrogen and has potential for large scale production.

1.2.3 CO_2 Transport

As mentioned above, global emissions need to be cut by six billion tonnes per year, and to achieve this goal infrastructure to support the transportation to the utilisation and storage sites must be in place. Due to the large magnitude a pipeline network where the CO_2 is pressurized is the best option to optimise the process. On the other hand, in the case of transportation from rural areas or of smaller quantities, transportation by ship where the CO_2 is liquefied has proven to be the most sustainable option. Transportation of pressurized gas and liquefied gas is an established technology in the Oil and

Gas sector, however the thermodynamic properties of CO_2 require more research, experimental data in particular, to be conducted in order to transfer the knowledge safely.

The main difference is that petroleum and natural gases can be liquefied at atmospheric pressure while CO_2 can only exist as gas or solid at atmospheric pressure. Thus, the pressure needs to be increased above the critical pressure of CO_2 (73.77 bar) where the density is at its highest. This is in the interest of the transporter as it maximises the capacity of the tank. The pressure is required to be maintained the critical point or above upon loading and offloading to avoid solid CO_2 (dry ice) from forming. There are yet to be produced CO_2 carrier ships of the same magnitude and capacity as liquefied natural gas and liquid petroleum gas as the ships produced in the past has been for CO_2 consumption purposes. This indicates there is a long way to go before this method of transportation is established and optimised.

As mentioned, for long-term projects of large magnitude transportation by pipeline is suitable (9). Norway has extensive experience with both transportation of hydrocarbons and CO_2 by pipeline. A company with extensive knowledge around transportation and storage is Equinor, being the sole operator of CO_2 injection wells with their two existing CCS projects at Sleipner and Snøhvit. They have a total injection rate of 1.7 million tonnes CO_2 /year.

As outlined, the solution varies depending on the application. Many times the solution is a combination of different technologies such as displayed in the Northern Lights project.
Northern lights handles the transportation side of the Longship project mentioned in chapter 1. The captured and processed CO_2 is transported from the Eastern part of Norway by ship to a reception terminal in Øygarden on the west coast of Norway. From here the CO_2 is transported to the offshore injection facility by pipeline.

A simple sketch of an example of a hybrid transportation chain is outlined in figure 1.3

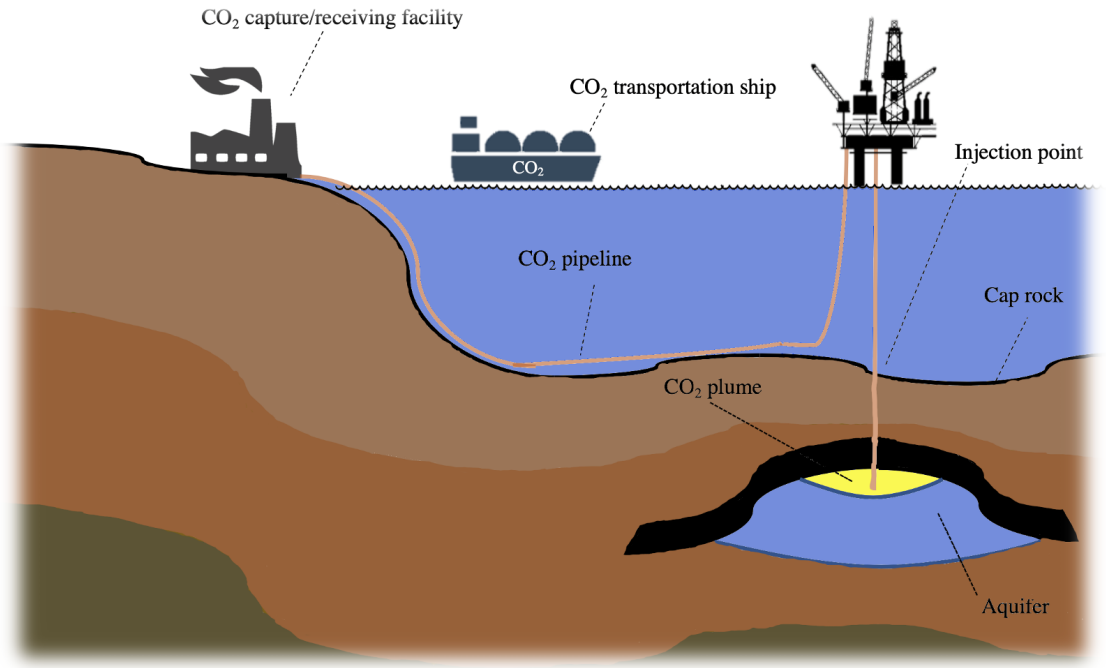

Figure 1.3:
CO_2 transport and injection sequence

1.2.4 Utilisation and Storage Solutions

There are several industries that require CO_2 as a product. This can range from decaffeinating coffee beans to being used as 'food' in greenhouses as it is necessary for photosynthesis. In this thesis, the focus will be aquifer storage due to relevance. Saline aquifers are common globally and are typically of large storage capacity. The Utsira formation on the Norwegian continental shelf is the sole saline aquifer used for permanent storage of CO_2 captured at the Sleipner field. This success confirms it is a viable option of formation for permanent storage. When evaluating a formation it is important to ensure the capacity is large enough to store the CO_2 required for the project or facilities life cycle. Equation 1.1, along with derivatives, are commonly used to evaluate the capacity of a field 1.1 (10).

$$m_{CO_2} = V_b \theta X \frac{Net}{Gross} \rho_{CO_2} \tag{1.1}$$

Where V_b is the bulk volume of the field, θ is the porosity, X is the storage efficiency factor, ρ_{CO_2} is the density of the CO_2 It is also important to evaluate the porosity and permeability to ensure it is of sufficient levels at the depth of the formation so that it provides a hydro-static pressure larger than the critical pressure. This ensures the storage site is maximised in potential as the liquid will remain at its high density with no vaporization. When the pure CO_2 is injected into the reservoir it is absorbed by the groundwater until it reaches its saturation point, and expected to sink further into the formation as a result of increased gravity of water when bound to CO_2 also referred to as convection. This will increase the capacity as the underlying brine will be pushed upwards. Experimental work is required to further understand and quantify the effect of different concentrations of salt and minerals, pressures and temperatures has on the diffusivity of the CO_2 into the brine.

1.3 Relevant Previous Studies

The first publication introducing an experimental method of determining the diffusion coefficient dates back to 1996. Riaziz developed a method where a pressurized gas column is in conctact with a WBS in an isolated system (11). The pressure of the system will decrease as CO_2 dissolves into the WBS, saturating the liquid until an equilibrium is reached. The model is made to represent the adsorption and desorption behaviour at operating conditions typical for CCS conditions. It proves to be an accurate and experimental method and the model has been cited several times when further research on CO_2 storage has been carried out, some mentioned in this chapter.

The method established by Riazi was adapted to high pressure systems to study the diffusivity of CO_2 in formation waters at ranging pressures and temperatures. Experiments and analysis was carried out by Zargham et al. different WBS. The findings of this study includes the increase of CO_2 diffusion at increased temperatures due to increased internal molecular activity. It also found the addition of salt lowers the diffusivity coefficient (12).

Farajzadeh et. Al compared the effective molecular diffusion and theoretical diffusion coefficient at a range of time intervals at high pressures (13). The measured effective molecular diffusion are fitted parameters of great importance when evaluating the transfer rate for CO_2 gas into a reservoir. The findings are that the diffusion coefficients for the short time interval measurements were highly inaccurate compared to the theoretical coefficient, by up to two orders of magnitude, while the experiments with long time intervals proved to be comparable. This result is evidence that convection accelerates the diffusion of CO_2 into WBS due to advection currents resulting from the increased density at the gas liquid interface.

To further understand the mass transfer mechanisms at the different stages of diffusion, a similar low pressure PVT experiment was carried out by Tungevik et al. where pH indicator was used to visualise the concentration changes and patterns(14). This further confirmed Farajazedehs results that convection contributes significantly to the high mass transfer coefficient at the intermediate mass transfer stage.

A range of pressure decay experiments were carried by Hansen as part of her master thesis. Both bulk volume and packed porous systems were tested, with saline and nonsaline WBS containing pH indicator. The visualisation along with pressure data obtained throughout the pressure depletion were used to develop diffusion coefficients. A simple pressure decay model was created for this purpose. The study provided valuable insight into understanding the contribution of the early and late time confection dominated diffusion of CO_2 into the solution (15).

Despite the experimental studies outlined above indicating concentration change through a pH indicator, it is not a sufficient method of quantifying the CO_2 absorbed in WBS in the PVT cell, hence determining the final saturated concentration at the saturated pressure, Psat. Being able to accurately quantify will give a better insight and understanding into the effect the condition has on the total absorption and desorption of the CO_2 gas in the WBS.

Through literature research done on the absorption/desorption process for polymer-based liquids in relation to pre-combustion CCT, it was noted that flash distillation of a pressurized water-based solution will remove the CO_2 present in the solution(16).Flash distillation effectively brings a pressurized system to atmospheric pressure, separating the gas and the liquid evaporated so that this can be quantified through either volume or weight. This is further backed up by the properties and solubility of CO_2 in water discussed in section 1.2.1 and 1.4.2. This study was as mentioned applicable

for polymer-based liquids so further research was carried out on flashing of saline and non-saline WBS.

Glade's article on Modeling of CO_2 release and the carbonate system in the Desalination journal refers to flash distillation of CO_2 from a WBS. The compositions used in the study are high compared to formation water, which we are trying to replicate. Despite different applications this research paper provides useful insight into the flash distillation of saline water containing dissolved CO_2 under pressure.

Professor Skule Strand and postdoc Ivan Dario Pinerez Torrijos at the department of Energy and Petroleum engineering at the University of Stavanger were consulted regarding using a flash cell paired with a gasometer to quantify the CO_2 absorbed by the WBS. It was agreed that this was possible to incorporate into the experiment as a method of quantifying the CO_2 absorbed. A similar method was used by Torrijos for flashing of CO_2 and saline water at high pressures, ranging from 50 to 250 bar. Utilising a gasometer of appropriate size and resolution with the flash cell will allow for flashing and accurate analysis of the gas, even at low pressures such as the saturated pressures, P_{sat} which is estimated at around 1.5 bar.

1.4 Underlying theory

1.4.1 Mass Transfer Mechanisms

Mass transfer is the quantity of a specific mass moving between the phase boundaries. It is important to study the mass transfer phenomenon's that take place for CO_2 and the knowledge is vital to the whole process cycle, from capture to storage.
Using a PVT cell the mass transfer of CO_2 in gaseous form into a WBS was studied. The aim is to accurately quantify the CO_2 absorbed by the liquid through flash distillation once the system inside the PVT cell has reached equilibrium at P_{sat}.

Interface interaction

As outlined in 1.2.1 the molecular structure strongly affects the properties of the compound. This also applies to the solubility of molecules. The H_2O molecule has a strong dipole moment due to the electron distribution in the covalent bond. As a result of this it is considered to be the superior molecule for dissolving substances. In fact, it is capable of dissolving a wider range of substances compared to any other liquid solvent. The molecular structure allows for hydrogen bonds to be formed and as a result the majority of substances with a polar structure will be soluble in H_2O. CO_2 on the other hand, like hydrocarbons, are non-polar. Figure 1.4 shows the molecular structure and distribution of the electrons of CO_2 and H_2O and highlights the non-polarity and polarity of the compounds respectively. Typically non-polar molecules will not dissolve in a polar solvent, however if the temperature and pressure of the system may alter the properties. To alter the solubility of gases increasing the pressure is effective while increasing the temperature is effective to alter the solubility of liquids and solids. Henry's law shows the relationship between the pressure of the gas phase above a liquid solution as a function of time

$$P(t) = K_H c(t) \tag{1.2}$$

K_H is Henry's law constant for a specific solute-solvent combination and is a temperature dependent variable with units $m^3 Pa/mol$. C is the concentration of the gas as a function of time with units $mol/m^3 3$. Henrys law shows the pressure of the gas phase is linearly proportional to the gas

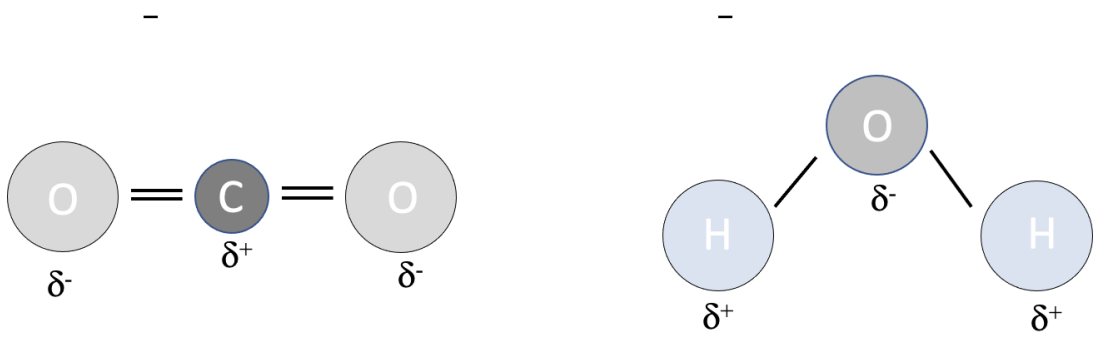

Figure 1.4: Chemical structure of CO_2 and H_2O

concentration at the interface between the solute and solvent until an equilibrium between the phases is achieved through diffusion.

Diffusion

As outlined in the previous chapter, differences in temperature, concentration and pressure will drive mass exchange until equilibrium between the two phases is reached. The mass transfer will move towards the lower energy state, which in our case is from the CO_2 gas phase to the liquid phase WBS. Diffusive flux is mass transfer due to random movement of particles. Flick's first law of diffusion is typically employed when the difference of concentration is the driving force for mass transfer in relation to displacement or time. In this case the concentration is changing with the displacement resulting in the following equation

$$\vec{J} = -Ddc(y)/dy \tag{1.3}$$

J is the flux of particles moving in direction y at the solvent-solute interface y=0 and has units mol/m2s. The diffusion coefficient a temperature dependent variable and is specific for the solute-solvent pair and is represented by D. As we have made the assumption the system inside the PVT cell is isothermic we can assume a constant value for the diffusion term. However, once the experiment commences the concentration will change as a result of the pressure decay. We therefore need to establish a relationship for the concentration distribution as the gas diffuses into the solution. The gas travels through the area of interface where molar mass transfer into the WBS occurs and causes a concentration change.

$$dn_{CO_2} = (J(y) - J(y + dy)) \tag{1.4}$$

$$dc(y) = \frac{dn_{CO_2}}{Ady} \tag{1.5}$$

J(y+dy) is equivilant to $J(y) + dJ(y) and J(y) = \vec{J}$ as we are limited to a one-directional system. Combining and simplifying equation 1.3 and 1.5 we get the following relationship for concentration change with respect to time in y direction:

$$\frac{\partial c(y,t)}{\partial t} = -\frac{\partial J}{\partial y} \tag{1.6}$$

Equation 1.6 is the first form of Fick's second law. J is then substituted from Fick's first law resulting

in the following term

$$\frac{\partial c(y,t)}{\partial t} = D\frac{\partial^2 J}{\partial y^2} \tag{1.7}$$

To predict the concentration change from diffusion with respect to time equation is the general solution from the diffusion equation if a one dimensional system is assumed (17). If wanting to solve the system with two dimension, the following equation can be employed.

$$\frac{\partial c(\vec{r},t)}{\partial t} = D\Delta^2 c(\vec{r}) \tag{1.8}$$

$\vec{r}$ is the position vector. It is important to note equation 1.12 is mathematically analogue to the heat equation. It is useful for evaluating convection driven flow, which is described and derived further in the following subsection

Convection

As previously established, changes in the density of fluid will further enhance the mass transfer. This phenomenon is referred to as convection and is a result of differences in temperature and pressure in the solution. An investigation of CO_2 gas into water is carried out and the following reaction occurs:

$$\begin{aligned} CO_2(g) &\Longleftrightarrow CO_2(aq) \\ CO_2(aq) + H_2O &\Longleftrightarrow H_2CO_3 \end{aligned} \tag{1.9}$$

When comparing the molecular weights of the products and solvent it is clear that the products are heavier than the solvent at isothermic conditions. The difference in density causes an instability in the solution due to gravitational forces acting on the system. Figure 1.5 illustrates the flow patterns caused by Rayleigh-Taylor instabilities. A 'mushroom' cap is formed due to the difference in densities of the fluids. This situation can be compared to the change in density caused by differences in temperature. The change in density can be described using a derived version of Boussinesq approximation;

$$\rho(T) = \rho_i(1 - \alpha\Delta T) \tag{1.10}$$

ρ_i is the density of the WBS at the ambient temperature, α is the thermal expansion coefficient and ΔT is the change in temperature To get a modified version where the change in density due to convection is derived by substituting the change in temperature with the change in concentration. This will be a precise method due to the direct relation between density and concentration.

$$\rho = \rho_i(1 + \beta\Delta c) \tag{1.11}$$

As the driving force is the concentration ρ_i becomes the density of the fluid at the reference point while $/beta$ is the coefficient of volumetric expansion. The Rayleigh number is modified according to this giving the following relation

$$Ra = \frac{\beta\Delta c r^3 g}{vD} \longrightarrow Ra = \frac{\Delta p r^3 g}{\rho_i vD} \tag{1.12}$$

Instabilities similar to described in this section are commonly affected by factors such as viscosity, surface tension, diffusivity and finite density gradients. The Atwood number, defined in equation 1.13, can be used to investigate the flow two fluids.

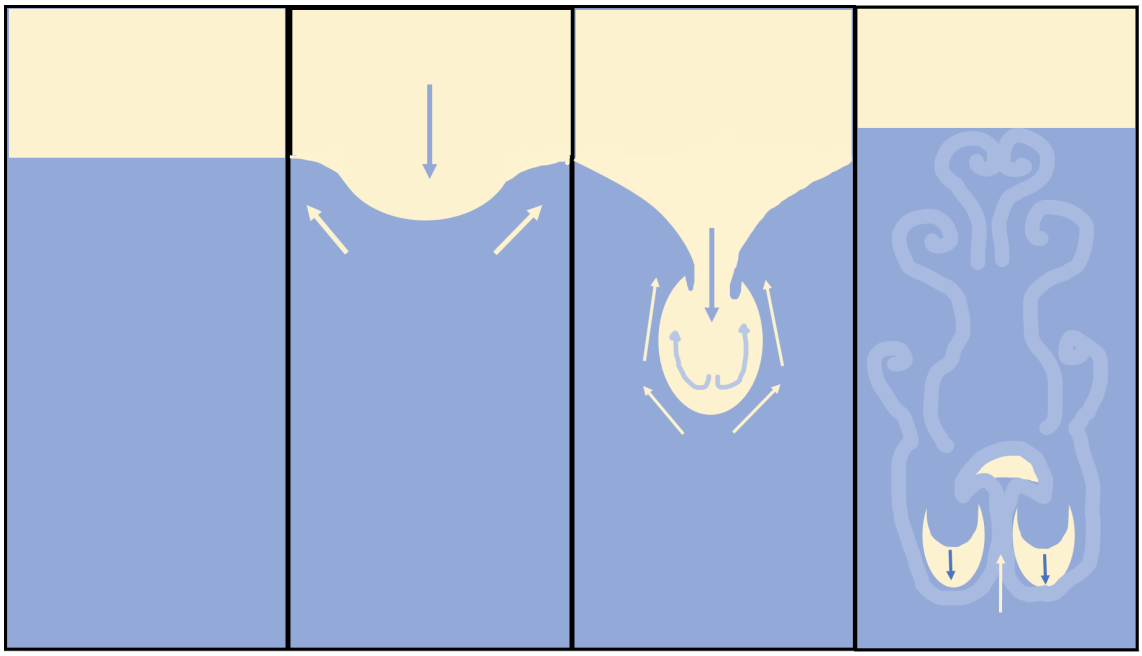

Figure 1.5: Rayleigh-Taylor instabilities causing convection due to gravitational forces

$$At = \frac{\rho - \rho_i}{\rho + \rho_i} \tag{1.13}$$

This expression is a simple ratio between two fluid densities. It describes the gravitational effects working on the denser and the effects of buoyancy working on the lighter (18). Low values of A_t indicate laminar flow and high values indicate turbulent flow.

1.4.2 Chemical solubility of CO_2

Dissolution with water

If gas concentration is considerably higher than the NaOH present in the water the following reaction occurs between the CO_2 and H_2O to produce bicarbonate ions.

$$CO_3^{2-} + H_2CO_3 \Longleftrightarrow 2HCO_3^- \tag{1.14}$$

The bicarbonate ions and carbonic acid comes to an equilibrium it will form a buffer mixture with the following reaction

$$CO_2^+ H_2O \Longleftrightarrow H_2CO_3 \Longleftrightarrow 2HCO_3^- + H^+ \tag{1.15}$$

The bicarbonate has a higher acidity so is considered the conjugate base. The buffer mixture of bicarbonate ions and carbonic acid prevents the pH from increasing significantly unless the magnitude of CO_2 dissolved reaches a point where the buffer capacity is exceeded. In this scenario the solution will become acidic and the solution will change colours if a pH indicator is used. The amount of CO_2 that can be dissolved in the water can be calculated and concentration change is driven by pressure. Reaction 1.14 and 1.15 is expected to occur but decelerates and become equal and stable in both gas and liquid phase. When this point is reached the system has reached its saturated pressure, P_{sat}, meaning mass transfer from the gas into the liquid stops.

Dissolution in saline solution

To more closely mimic the diffusion of CO_2 into formation water upon injection, like pictured in figure 1.3, saline WBS were used. Naturally compositions of formation waters change depending in the surrounding geology, however subsea aquifers suitable for permanent storage have high levels of dissolved solids. A saline solution at standard brine composition was therefore considered to be an appropriate concentration. The results obtained using the standard WBS and WBS + NaCl can be compared to investigate the effects of increased levels of ions in the solution. For the saline WBS 38.4 g/L of NaCl was added, providing an ionic strength of 0.657 M.
Instead of directly reacting with the H_2O molecules, the NaCl dissociate into ions;

$$NaCl \longrightarrow Na^+ + Cl^- \tag{1.16}$$

As previously discussed in subsection 1.4.1, H_2O is the greatest known solvent due to their high polarity. Its ability to dissolve components and impurities are further enhanced through increased pressure and temperature. When adding the salt the water becomes more viscous as the ions are hydrated. It is therefore expected to see some reduction in solubility when adding salt (19)

Alkaline Solutions

The addition of ionic hydroxide compounds to water results in an alkaline solution. It increases the pH of the solution to a value greater than 7, depending on the magnitude added, and occurs due to the increase of OH- (aq) in the system. As strong bases have the ability to completely dissolve in water it will ionise into hydrogen and hydroxide ions and their corresponding anion. When the CO_2 is injected in the system with an alkaline WBS it will form sodium carbonate salt from reacting with the excess base in the solution. This is displayed in the following chemical reaction

$$CO_2 + 2NaOH \Longleftrightarrow Na2CO3 + H_2O \tag{1.17}$$

Despite not being acidic independently CO_2 becomes slightly acidic when dissolved in a WBS. Reactions between acids and bases depends heavily on the concentration of the base present in the solvent as it is directly related to the ability to dissolve into OH- **??**. This means that dissolution of gas at small magnitudes will not significantly effect the pH due to the alkalinity of the sodium hydroxide. With this in mind the amount of NaOH added to the solution was kept minimal in order to serve its purpose to increase the initial alkalinity for visual effects without implicating the reactions occurring. The small amount of sodium carbonate salt produced at the interface initially will contribute to the alkalinity of the WBS. Despite the NaOH present and their effect on the system, the concentration is low compared of the concentration of CO_2 gas present. Therefore the concentration of NaOH can be considered negligible and are not evaluated or elaborated on further.

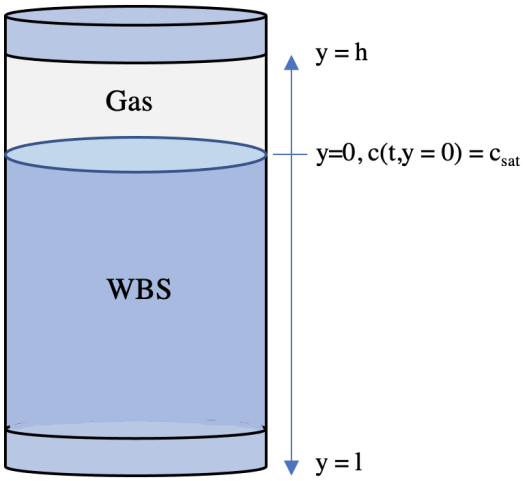

Figure 1.6:
Simplified model of the PVT cell containing a gas and liquid column.

1.5 Analytical derivation

A simple model of the PVT cell is derived for further understanding and measuring of the diffusion process in the system. The boundaries are implemented to keep the calculations simple while maintaining accuracy compared to the experimental measurements. The experiment is limited by the equipment, therefore the pressures will not exceed 7 bar. When comparing the real behaviour of CO_2 to what the ideal gas is predicting for the pressure range used for the calculation the discrepancies will be minimal(20). However, for the sake of comparison two methods are employed when calculating the concentration for the mass balance. The second method of calculating the pressure is Van der Waal's equation. It is a derivative of the ideal gas law and will be further outlined in the mass balance section later in the chapter.

Implemented boundary conditions

Diffusion is assumed to be the dominant mass transfer mechanism in to a finite liquid height column. Figure 1.6 shows the model of the cell at t=0. The following boundary conditions apply; The system consist of a CO_2 gas cap at initial pressure, $P_i = P(t = 0)$, which has to be over atmospheric pressure, $P_i > 1.013$ bar. The CO_2 is on top of a column of WBS. To simplify the derived the model the change of density only change as a function of time due to the pressure decay. This means we assume the contribution of water vapour from phase change from liquid to gas are negligible despite the saturation pressure of water being at 25 °C and 0.0317 (21), which is within the range of conditions we are operating in. Furthermore, this means the boundary between the phases is constant and swelling of the solution when CO_2 is dissolving is disregarded. To describe the gas behaviour of CO_2 the real gas equation is employed as displayed in 1.18

$$PV = Zn_{CO_2}RT \tag{1.18}$$

Z represents the gas compressibility factor and is assumed constant at 0.98. The P_i t=0 the phases are considered completely separated, except the interface part of the solution which is assumed saturated with CO_2 instantaneously. This means that the CO_2 concentration is zero at t=0 in between the boundary of the liquid phase ($0 < yL$) and maximal at the boundary $0 < y < h$ and c_sat is is defined by

the initial gas pressure, P_i.

$$\begin{aligned} &= c(t, y = 0) = c_{sat} = P_{sat}/K_H \\ &= c(t = 0, y > 0) = 0 \end{aligned} \tag{1.19}$$

Equation 1.19 shows the direct correlation between c and P, which allows for the derivation of the mass flux of the gas CO_2 (g) $\longleftrightarrow$ CO_2 (aq) at the interface, y=0:

$$n_{CO_2}(t) = \frac{V}{zRT}(P_i – P(t)) \tag{1.20}$$

n_{CO_2} can be determined by the gas column pressure at $t > 0$. Differentiating the previous equation with respect to time and by rearranging with equation 1.4 the following term is obtained:

$$\frac{dn_{CO_2}(t)}{dt} = \frac{V}{zRT}\frac{dP(t)}{dt} = -JA \tag{1.21}$$

Where J is obtained from Flicks first law displayed in equation 1.3. The change in pressure is described by Henry's law displayed in equation 1.2. It was previously assumed the gas volume at the cross sectional area is constant, hence the gas volume and area can be simplified to the height of the gas, h. This gives the following relation at the interface;

$$\frac{dP(t)}{dt} = \frac{-zRTD}{h}\frac{dc(t, y)}{dy} = 0 \tag{1.22}$$

The upper boundary required to analytically solve Fick's second law of diffusion is displayed in equation 1.43. It relates downwards concentration increase by flux with the parameters pressure and time.

Gas Concentration derivation

As stated the initial concentration of CO_2 in the WBS is assumed to be zero at t=0. At the interface, y=0 the top of the WBS column is instantly saturated when the experiment is started. As diffusion process commences, a rapid decrease in pressure is expected before the top layer of the WBS is fully saturated and turns into CO_2 in aqueous form. The CO_2 (aq) is heavier than the WBS the convection driven transfer mechanism be the primary mass transfer driving force due to the mixing throughout the whole length of the column, $(0 < y < L)$.
Fick's second law, referenced in equation 1.3 , is a one dimensional partial differential equation (PDE). It is a linear relationship with a constant coefficient specified for the system. It can be solved by applying the boundary conditions specified through Fourier analysis. The method of separation of variables gives the following function for the product;

$$D(t, y) = f(t)g(y) \tag{1.23}$$

Substituting above equation into flicks second law, equation 1.3 and divide by f and g on both sides of the equation the following differential equation is obtained;

$$\frac{1}{f}\frac{df}{dy} = \frac{D}{g}\frac{d^2g}{dy^2} \tag{1.24}$$

For the time and displacement variables to be evaluated independently both sides of the equations need to be constant This is achieved through rewriting both sides of the equation with regards to the positive constant, T, as the left side of the equation has the dimensions of t^-1. By also accounting for the

diffusion exponentially decaying the following equations are obtained for the time and displacement.

$$\frac{1}{f}\frac{df}{dy} = \frac{1}{\tau} \longrightarrow \frac{df}{dy} = \frac{1}{\tau} \tag{1.25}$$

$$\frac{D}{g}\frac{d^2g}{d^2y} = \frac{1}{\tau} \longrightarrow \frac{d^2g}{d^2y} = \frac{g}{D_\tau} \tag{1.26}$$

The term for time, equation1.25, is a familiar first order linear ordinary differential equation (ODE) for exponential growth or decay and has equation 1.27 as its solution

$$f(t) = f(0)exp(\frac{-t}{\tau}) \tag{1.27}$$

f(0) is obtained from the initial data when t=0.
The term for displacement, equation 1.26 is solved like a simple harmonic oscillator where the wave number, K, equals D_τ^-1 and is displayed in equation 1.28:

$$g(y) = g_1 cos(\kappa y) + g_2 sin(\kappa y) \tag{1.28}$$

g_1 and g_1 are determined from the boundary conditions and are constant. To satisfy the boundary at the initial conditions, g=0 at the upper boundary y=0 must equal zero. This is also the case for the derivative for the concentration term, which must equal zero at the bottom of the cell, y=l. Thus, κ will be zero only in specific cases;

$$\kappa_m = (2m+1)\frac{\pi}{2L} m = -|N \tag{1.29}$$

Which implies the following expression for τ

$$\frac{1}{\tau_m} = D\kappa_m^2 = D((2m+1)\frac{\pi}{2L})^2 \tag{1.30}$$

Applying the method of separation of variables to Flick's second law gives infinitely many distinct solutions with the boundaries defined in the previous section. The following definition for Fourier mode the expression of the function product is established in equation 1.31.

$$c(t,y) = a_m exp\frac{-t}{\tau_m)} sin(\kappa_m y) \tag{1.31}$$

Based on Fick's second law being linear, equation 1.32 is the most general solution to the previous expression. It is a superposition of a superposition of the infinite specific solutions.

$$c(t,y) = a_0 + \sum_{n=0} a_n exp(\frac{-tD(2n+1)^2\pi^2}{4L^2}) sin(\frac{(2n+1)\pi y}{2L}) \tag{1.32}$$

The following initial boundary condition is applied at t=0;

$$C(t, y=0) = a_0 = c_s at \tag{1.33}$$

The gas concentration in the area $0 < y < L$ at t=0 gives the following expression for a_n:

$$\int_0^L c(t=0,y)dy = a_n = -a_0 \frac{4}{(2n+1)\pi} \tag{1.34}$$

$$c(t,y) = c_{sat} + \sum_{n=0} c_{sat} \frac{4}{(2n+1)\pi} exp(\frac{-tD(2n+1)^2\pi^2}{4L^2}) sin(\frac{(2n+1)\pi y}{2L}) \tag{1.35}$$

Equation 1.35 is the final expression for the gas concentration as a function of time and solution depth. A full derivation of an can be found in appendix A.

Diffusion coefficient

To calculate the mass transfer precisely a different diffusion coefficient must be derived, namely for the early and late stage diffusivity.
Integrating the upper boundary term specified in equation 1.22 gives the change in pressure caused by diffusion;

$$\int_{P(t)}^{P_{sat}} dP(t) = \frac{-zRTD}{h} \int_t \frac{dc(y)}{dy}|_y = 0 \tag{1.36}$$

The concentration at the interface can be described if the gas concentration term, equation 1.34, is differentiated with respect to the displacement, y.

$$\frac{dc(t,y=0)}{dy} = -\sum_{n}^{\infty} c_{sat} \frac{2}{L} exp(\frac{tD(2n+1)^2\pi^2}{4L^2} \tag{1.37}$$

If we substitute this into the pressure change by diffusion term, equation 1.37 and integrate over the domain, we obtain the following relation:

$$P(t) - P_{sat} = \frac{8LzRT}{\gamma\pi^2} c_{sat} \sum_{n}^{\infty} \frac{1}{(2n+1)^2} exp(\frac{tD(2n+1)^2\pi^2}{4L^2}) \tag{1.38}$$

Where γ is LzRT/h.
Reformulating this relation with consideration of the real gas law, equation 1.18 at the upper boundary gives the following equation for determining the pressure differences;

$$P(t) - P_{sat} = \frac{8}{\pi^2}(P_i - P_{sat}) \sum_{n}^{\infty} \frac{1}{(2n+1)^2} exp(\frac{tD(2n+1)^2\pi^2}{4L^2}) \tag{1.39}$$

Analytically solving equation 1.39 shows that with time the pressure will converge towards a single value as $t- > \infty$. This value is determined by evaluating the equation at $n = 0$, giving the following term;

$$P(t) - P_{sat} = \frac{8}{\pi^2}(P_i - P_{sat}) exp(\frac{tD\pi^2}{4L^2}) \tag{1.40}$$

At this point we are able to finally determine D by applying the natural logarithm to both sided of the pressure equation and inserting the values obtained from the experimental data.

$$ln(\frac{P(t) - P_{sat}}{P_i - P_{sat}}) = \frac{8}{\pi^2} tD\pi^2 4L^2 \tag{1.41}$$

As $t- > \infty$ the solution will be saturated with CO_2 meaning no more gas is able to diffuse into the solution. To find the saturation pressure the law of mass conservation is applied to Henry's law and the real gas law as shown in the following equation;

$$P_{sat} = \frac{P_i K_H h}{K_H h + zRTL} \tag{1.42}$$

The relation is identical to the one obtained by Hansen (15).

1.5.1 Overall mass balance of CO_2 in and out of the system.

By quantifying the gas entering and exiting the PVT, as well as the gas remaining in the PVT cell after the saturation pressure is reached, a complete mass balance for CO_2 in the system can be carried out.

$$n_{in} = n_{sat} + n_{fl} \tag{1.43}$$

The although a pressurized gas, meaning the ideal gas law can typically not be applied, the pressures used in can be considered low enough that according to a graph the American Society of Chemical Physics , the gas tends to follow the ideal gas law at these pressures, where the discrepancy increases as a function of increasing pressure(22). From the experimental temperature and pressure the moles of CO_2 injected into the PVT cell, n_{in}, can be calculated using the ideal gas law with the compression factor specified earlier.
An alternative is to use Van der Waals equation, displayed in equation 1.44. The equation is a modified version of the ideal gas law, equation 1.18, taking intermolecular forces and molecular size. The CO_2 remaining in the gas pocket can be quantified using the same equation.

$$(P + \frac{an^2}{V^2})(V - nb) = nRT \tag{1.44}$$

Where a and b are empirical constants specific for each gas with the values and units $3.610\, L^2atm/mol^2$ and $0.0429\, L/mol$ respectively at $279°K$. The temperature is assumed to be the same as the ambient temperature which is consistently around $279°K$.
The equation can be rearranged to determine the number of moles present in the system. For the gas at t=0, the following equations will apply for the real gas law and Van der Waal's equation respectively

$$n_i = \frac{P_{in}V_{gp}}{RT} \tag{1.45}$$

$$n_i = \frac{V_{gp}^2(-\sqrt{\frac{4abP_i}{V_{gp}^2} + (\frac{a}{V_{gp}} - RT)^2} - \frac{a}{V_{gp}} + RT)}{2ab} \tag{1.46}$$

Where P_i is the initial pressure at t=0, V_{gp} is the volume of the gas pocket in the PVT cell which is constant.
Similarly, the remaining gas when the saturation point is reached can be quantified from equation 1.48

$$n_{sat} = \frac{P_{in}V_{gp}}{RT} \tag{1.47}$$

$$n_s = \frac{V_{gp}^2(-\sqrt{\frac{4abP_{sat}}{V_{gp}^2} + (\frac{a}{V_{gp}} - RT)^2} - \frac{a}{V_{gp}} + RT)}{2ab} \tag{1.48}$$

Inputting the exp in the experimental data into equation **??** and 1.48 gives the number of moles introduced and remaining in the system respectively.
To quantify the CO_2 gas dissolved into the WBS a flash distillation column with a gasometer attached is utilised to determine the moles of CO_2 leaving the system. As the gas is flashed to atmospheric pressure the ideal gas equation, equation 1.18, can be assumed valid. By applying the appropriate paramters equation 1.49

$$n_{fl} = \frac{P_{atm}V_{gas}}{RT} \tag{1.49}$$

By combining the equations above a full mass balance can be obtained.

$$\frac{V_{gp}^2(-\sqrt{\frac{4abP_i}{V^2}+(\frac{a}{V_{gp}}-RT)^2}-\frac{a}{V_{gp}}+RT)}{2ab} - \frac{V_{gp}^2(-\sqrt{\frac{4abP_{sat}}{V^2}+(\frac{a}{V_{gp}}-RT)^2}-\frac{a}{V_{gp}}+RT)}{2ab} - \frac{P_{atm}V_g}{RT} = 0 \tag{1.50}$$

1.5.2 Remaining CO_2 after flashing

Despite having established that CO_2 typically does not dissolve in water at atmospheric pressures, precautions were taken to account for any CO_2 remaining in the liquid after flashing. The density of the WBS is recorded before and after the experiment runs. From (23) Garcias publication on density of aqueous solution containing dissolved CO_2 we obtain equation 1.51, allowing for the concentration to be determined through rearranging.

$$\rho_{sat} = \rho_1 + M_2 \cdot c - c \cdot \rho_1 V_\phi \tag{1.51}$$

Where ρ_{sat} is the density of the CO_2 saturated liquid ρ_1 is the measured density before saturating the liquid with CO_2 , M_2 is the molecular weight of CO_2 , V_ϕ is the apparent molar volume. V_ϕ is determined through the polynomial fit displayed in equation 1.52

$$V\phi = a + b \cdot T + c \cdot T^2 + d \cdot T^3 + e \cdot T^4 \tag{1.52}$$

Where T is the temperature and a, b, c, d and e are correlation constants. The constant varies with literature, but for this work Garcia's constants are used to stay consistent.

Chapter 2

Methodology

Different experiments were carried out in bulk volume with different gas-liquid ratios and initial pressures. Both saline and non saline alkaline water-based solutions were used as the liquid phase and pressurised CO_2 was used as the gas phase.

2.1 Experimental setup

Pressure decay of a gas-liquid system in a non-invasive PVT-cell of fixed volume. The cell is encased in a cuboid epoxy block. The cuboid shape is utilised to eliminate visual phenomenon and disturbances typical for cylindrical shapes. The epoxy block is assumed to insulate the cell and the system is therefore considered isothermal. The cell has an internal diameter of 66 mm and has a volume of 1380 ml. Injection and extraction can be done from the both top and bottom of the cell. The three-way valve at the top of the cell controls the CO_2 gas inlet from the pressurised tank and is connected to the PASCO Absolute Pressure and Temperature sensor. The sensor transmit signals that are communicated to a computer through the Pasco 850 Universal Interface monitor. As seen in figure 2.1 the temperature probe is outside of the cell, hence a non-invasive cell, to ensure consistency in the ambient temperature. Similar to the top of the cell, the bottom also has a three-way valve connected to a liquid extraction tube, leading to a bucket collecting the waste fluid from flushing the cell, and a tube leading to the flash distillation column for further analysis.
The flash column is connected to a 50 ml burette placed upside down in a 5 L water beaker. The valve installed at the top of the burette can be opened and closed to control the vacuum inside the burette. A suction balloon was used to adjust the level the liquid to the tare value between each experiment. The CO_2 flashed from the WBS exits the tube leading inside the burette, the gas will travel to the top, pushing the liquid down and out of the burette. The discrepancy of the height of the water gives the amount of gas desorbed from the WBS.
Pressure tests of the system was carried out after opening the cell for cleaning or other maintenance to ensure no leaks in the system

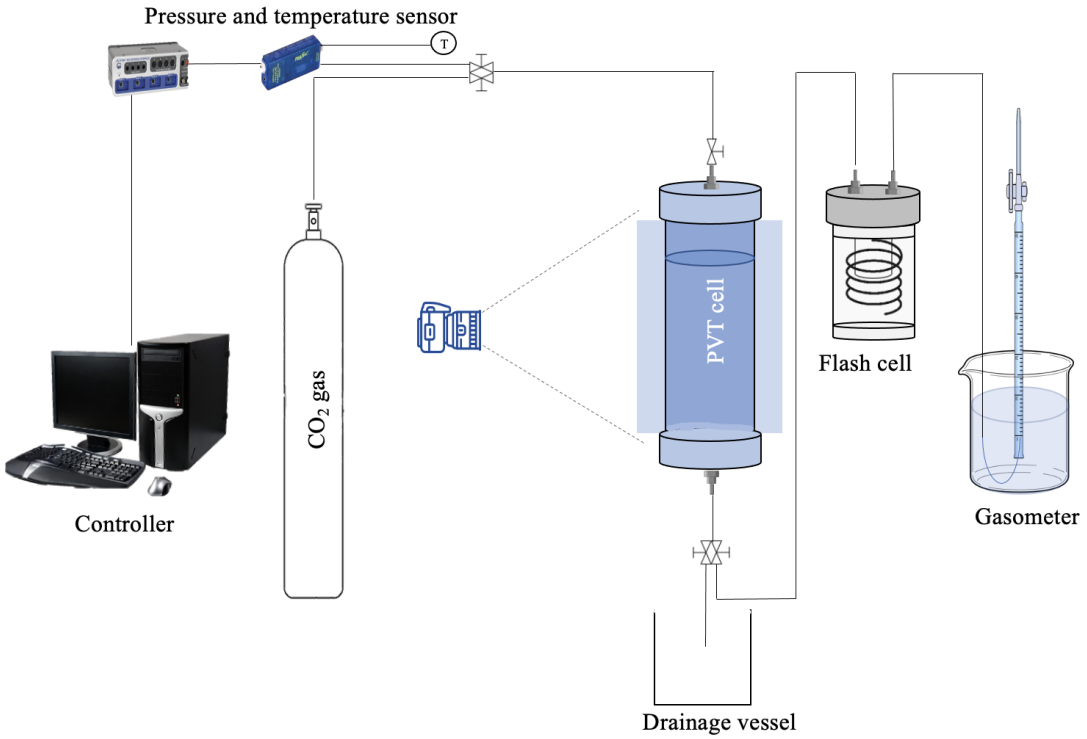

Figure 2.1: Experimental components of the PVT cell and flash distillation setup

2.2 Experimental procedure

A set volume of WBS was extracted from the bottom of the cell and while the same volume of CO_2 is injected into the cell simultaneously. The CO_2 injection continues until the pressure reaches around 7 bars. The system is then sealed off and interactions between the CO_2 gas and WBS commences. There will be a pressure reduction due to mass transfer from gas to liquid. Changes in temperature and pressure are monitored by Pasco Absolute Pressure and Temperature sensor. To observe the visual phenomenon's a camera was photographing the process at set time intervals.
For the experiment there were many steps of analogue nature that need to be carried out quickly to ensure an accurate experiment, hence results. To eliminate or limit human error it was written out a step by step procedure for each aspect of the experimental procedure. A complete detailed set of experimental procedures can be found in appendix C.

2.2.1 Solution composition

From the previous chapter we have outlined the mass transfer mechanisms expected for the CO_2 and WBS. In order to visually observe the mechanisms the WBS was prepared as an alkaline solution with a pH level of 11. The following table lists the components that make up the solution base recipe.
The Sodium hydroxide is added to alter the pH level of the solution. Bromothymol blue is added as the pH indicator and is chosen as the impact it has on the alkalinity of the solution is negligible. To ensure accuracy each mixture made up was measured with a METTLER TOLEDO SevenCompact pH-meter. The method for this along with the experimental data can be found in appendix D and E respectively.

Table 2.1: Composition of saline and non-saline WBS.

	Non-saline WBS		Saline WBS	
Deionised water	5.00	L	5.00	L
Sodium hydroxide	8.00	mL	8.00	mL
Bromothymol blue	35.00	mL	35.00	mL
Salt NaOH	0	g	193.50	g

2.2.2 Flash Distillation

Once the bulk volume part of the experiment had reached equilibrium, hence a WBS fully saturated with CO_2 , flash distillation was carried out to quantify the amount of CO_2 desorbed from the WBS upon pressure release from the saturated pressure, P_{sat}, to atmospheric pressure, 1.018 bar.
The flash cell was connected in order to quantify the CO_2 absorbed by the WBS. The volume of liquid flashed was calculated using the density equation 2.2. As mentioned in the experimental procedure the quantity of CO_2 gas To scale up amount of CO_2 from the WBS used for flashing to the WBS in the PVT cell a simple ratio was used as a scale up factor as shown in equation 2.1

$$SF_{WBS} = V_{flashed}/V_{PVTcell} \tag{2.1}$$

The individual scale up factor was applied to each experiment and an overview can be found in appendix G.

2.2.3 Density and SG measurements of WBS

To accurately determine the density of the WBS a D M A 4100 Density meter by Anton-Paar was employed. The density meter only required a small amount of the WBS to give highly accurate results. The definition of density displayed in 2.2is used as the base of the analysis. An overview of the densities obtained before and after running the experiment can be found in appendix F.

$$P = m/V \tag{2.2}$$

The apparatus contains a U-shaped borosilicate glass tube vibrating at a set frequency. Through precise determination of the characteristic frequency and carrying out a mathematical conversion the density of the WBS is found. The density will be important when carrying out mass balances and the remaining CO_2 as outlined in chapter 3.2.

Chapter 3

Experimental results

The procedures outlined in chapter 2 were carried out to observe the diffusion of CO_2 into a WBS until P_{sat} was reached. Once saturated the amount of CO_2 absorbed by the WBS through flash evaporation. Throughout the time the experiments were carried out a total of 25 experiments, though where most were repeated due to modification to the method throughout. The addition of the flash-cell was the cause of the ongoing modification of the method. Since the method was derived from applications at much higher pressures it had to be tuned to have appropriate physical parameters such as the gasometer resolution.
Problems related to leaks were also common source of compromised, hence unusable experiment data. In many cases the leak was detected early in the experiment by observing auditory cues or the data obtained from the pressure transmitter in real time, seeing a quick drop in pressure. In some cases the leak was too small to be detected early in the experiment and would only be noticeable when the pressure had dropped to atmospheric pressure, P_{atm} as apposed to the saturated pressure, P_{sat}. In the case of a leakage the PVT cell was disconnected from the rest of the apparatus. The PVT cell was then pressure tested using the procedure outlined in Appendix C.
As the PVT cell had been damaged from previous use at pressures higher than the limitation of the cell, the pictures will show yellow stains on the back of the cell. This is a a pocket where the WBS has seeped into through the crack when the. The pocket around the sealed crack is negligible in size and the liquid is still concealed in the system. Therefore this fault in the cell is not considered to effect the results, other than being slightly disturbing for the visualisation of the mass transfer displayed in figure 3.11 and 3.11.

3.1 Pressure data

3.1.1 Non-saline WBS

An overview of the experiments carried out with non-saline WBS is displayed in table 3.1. The initial pressure, P_i, was a changing variable between the different experiments. This was done to observe the effect the P_i had on the mixing regime, saturation time, diffusion coefficient and the amount of CO_2 absorbed when the saturated pressure, P_{sat}, was reached. The gas/liquid ratio was kept as constant as possible, however manual opening and closing of the valve caused some human inconsistencies. This has been accounted for in the calculations, and the volume of gas and liquid is measured individually and

	Pressure (P_i)	Gas/Liquid Ratio	Henry's constant	Temperature ($°K$)
Experiment 1	6.10	0.38	3623.53	296.19
Experiment 2	5.50	0.39	3622.41	296.28
Experiment 3	4.50	0.38	3621.83	296.12
Experiment 4	4.30	0.38	3622.52	296.17
Experiment 5	3.50	0.38	3621.52	296.27

Table 3.1: An overview of experiments carried out with non-saline WBS.

specified for each equation. The temperature remained almost constant, ranging between 23.5 -24.5 $°C$. As mentioned in chapter 2 a temperature transmitter was used to obtain data for more accurate calculations.

Figure 3.1 shows the pressure decay data for the full range of P_i using non-saline WBS. The theoretical saturated pressure, P_{sat}, has been added as a reference.

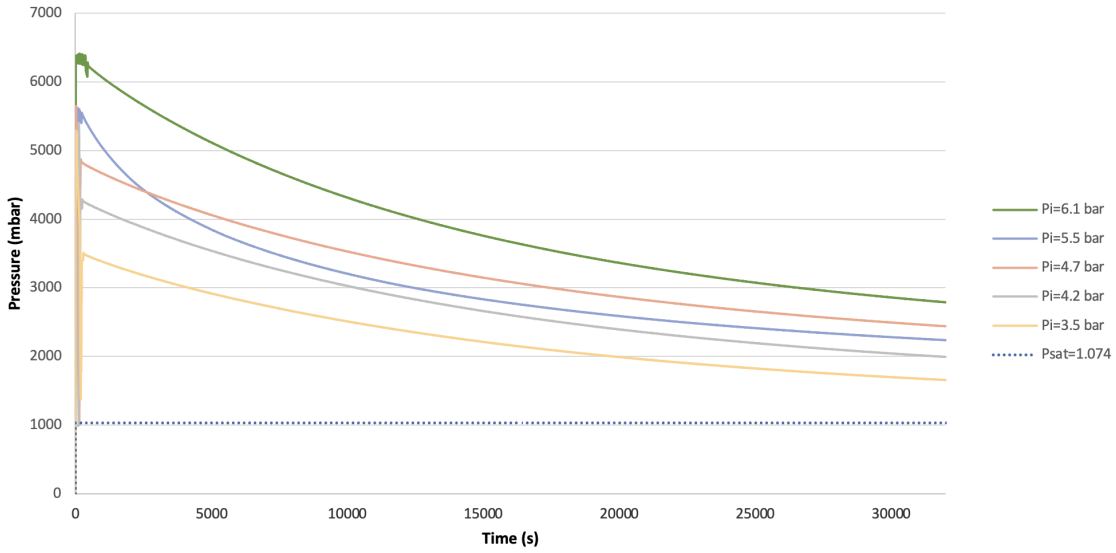

Figure 3.1: Pressure decay data for non-saline WBS

The experiments with a initial pressure less than 5.70 bar gave a saturated pressure, P_{sat}, less than the atmospheric pressure, 1.018 bar. This suggests the system is in vacuum which is not possible in this scenario. It is suspected the model is not valid as the pressures investigated in the experimental work are too low to estimate.

The model can therefore be disregarded for experiment 2-5. It is noted that the magnitude of the experimental saturated pressures are consistently higher than predicted by the model. This can be as the gas/liquid ratio is too high, which is further backed up by the mass balance discussed in chapter . However this should be accounted for by the terms for the PVT cell height, L, and gas column height, h. Although proven that the model does not predict accurate saturated pressure at the range used for this study, it is not fair to disregard the model. While not accurate, the results show close relations to the behaviour of the saturated pressure as a function of time and may be appropriate for experiments with higher pressures.

The figure shows a similar pressure decay trend, where the pressure depletion rate is fast for the first hours then proceeds to decelerate towards $y =$. This is evidence of the convection enhancing the mass transfer rate and agrees with the findings of Farajzadeh and Hansen (13), (15).

Experiment 2 with $P_i = 5.5bar$ shows a more rapid pressure depletion rate and has a P_{sat} lower than experiment 3 where $P_i = 4.8bar$. This indicated there was a minor, yet significant undetected a leak. It is also noted that it is the only experiment where the P_i and P_{sat} are not directly proportional, as the P_{sat} falls below the P_{sat} for experiment 3. Therefore the results from experiment 2 will not be evaluated further.
The dotted line is the P_{sat} calculated from equation 1.42. It is clear the real experimental pressure is significantly higher than the one obtained through the derived expression. This was expected as the P_{sat} calculated for experiment 2-5 were lower than the atmospheric pressure and is further evidence the model is not as precise as predicted for this case. It also agrees with Hansen's findings (15) obtained using a PVT cell with identical parameters. It is suspected the model is not accurate at the low pressures used for the experiment due to the limitations of the equipment. It is important to note that if thw experiment was repeated at higher pressures, Van der Waal's equation should be substituted for the real gas law to account for the difference between CO_2 's thermodynamic predictions by the real gas behaviour and Van der Waal's the discrepancies increases as a function of pressure.

3.1.2 Saline WBS

Table 2.1 shows an overview of the experiments carried out with NaCl added to the WBS. This was done to investigate the effect of increased ion concentration and apply the results to saline aquifers. As addressed in the literature research an increase in hydration of ions and increased viscosity will inhibit the rate of enhanced diffusion in the PVT cell.
Due to time limitations and limited access to BTB the sample size was changed from 5 to 3. The P_i from experiment 1, 3 and 5 were attempted to be replicated, however the CO_2 bottle had an analog gauge and the pressure was set manually. This proved to be somewhat inconsistent, but while not completely identical, results were obtained around the same P_i as the non-saline experiments. The theoretical saturated pressure was again less than atmospheric pressure when evaluating the lower pressures, therefore it is disregarded for experiment 7 and 8.

Table 3.2: An overview of experiments carried out with saline WBS.

	Pressure (P_i)	Gas/Liquid Ratio	Henry's constant	Temperature (°K)
Experiment 6	6.10	0.38	3623.53	296.19
Experiment 7	4.50	0.39	3623.53	296.38
Experiment 8	3.30	0.38	3623.53	296.87

Figure 3.2 shows the pressure decay data for the full range of P_i using saline WBS. The theoretical saturated pressure, P_{sat}, for experiment 6 has been added as a reference.
Figure 3.2 displays the pressure
The first notable phenomenon is the identical pressure depletion of experiment 6 and 7. A similar trend was not apparent in the non-saline WBS experiments. This comparison is not fair as we have already stated that the results from experiment 5 are compromised. If time and resources allowed a repetition of experiment 5 would give a better insight into the correlation between experiment 6 and 7 to determine whether it is a phenomenon that repeats itself or if the data for experiment 6 is compromised. It is possible the high pressures will increase the diffusion rate followed by converging and deceleration towards a pressure uniform depletion curve approaching P_{sat}.As the figure shows data over 9 hours the initial it is difficult to determine the early behaviour. The early pressure data will be addressed later in the chapter where it is compared to the visual time series of the experiment.

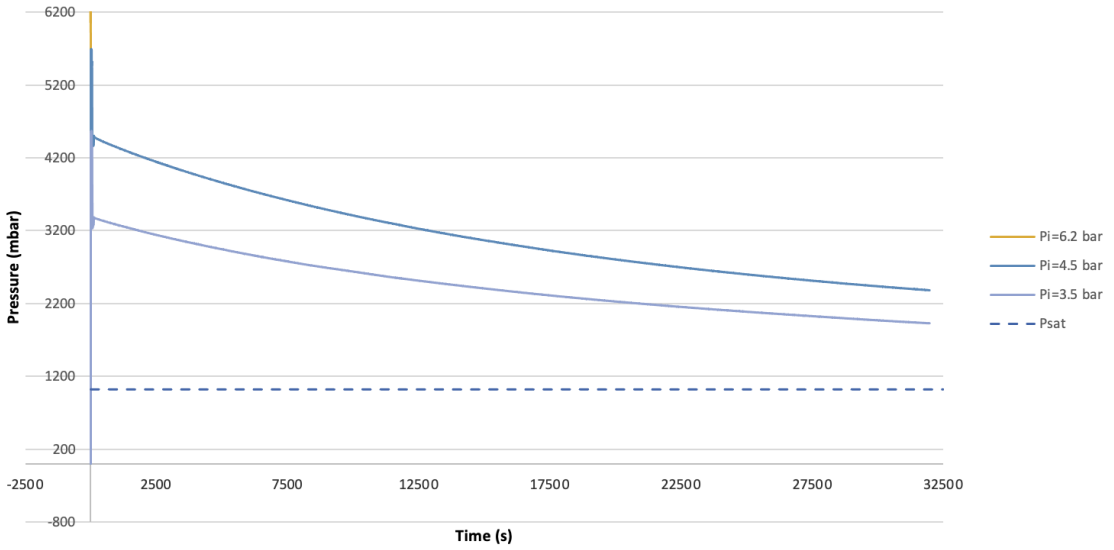

Figure 3.2: Pressure decay data for saline WBS

3.1.3 Non-saline and saline comparison

Figure 3.3 and 3.4 show a comparison of pressure decay data for 3.5 bar and 4.5 bar respectively.

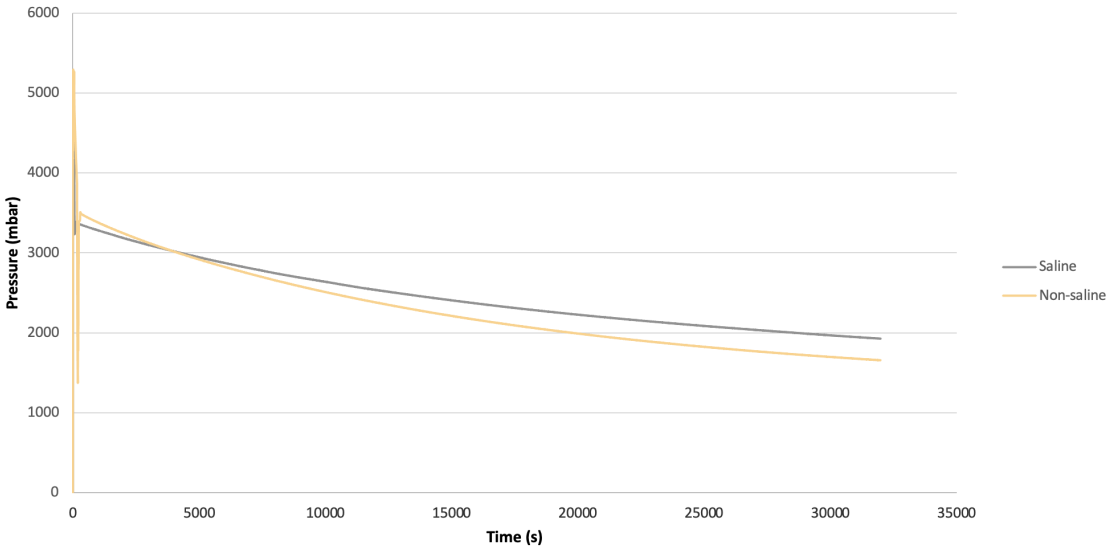

Figure 3.3: Pressure decay data comparison for non-saline and saline WBS at Pi=3.50 bar

Figure 3.3 shows that the pressure depletion rate is lower and P_{sat} is higher for the saline WBS compared to the non-saline WBS. This proves that even at low salinity's, the effect of NaOH and increased ionic hydration is evident. This suggests the inhibiting effect of salt lowers with increase of pressure. The same can be observed in figure 3.4. As mentioned the P_i was difficult to set accurately, and the P_i is therefore slightly higher for experiment 7. At first glance this can give the illusion that experiment 7 has a higher diffusion rate as it has a lower P_{sat} compared to experiment 3. When investigating the graph more closely it is clear the diffusion rate is lower for the saline WBS. From both comparisons it is clear the concentration of salt is significant and effects the solubility of CO_2 .

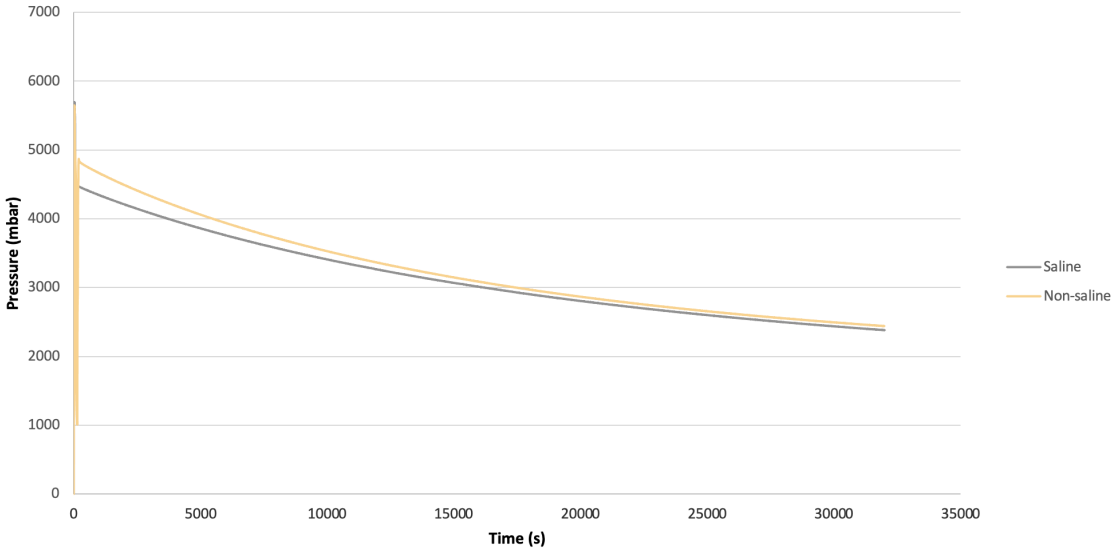

Figure 3.4: Pressure decay data comparison for non-saline and saline WBS at Pi=4.50 bar

Diffusion coefficient

The method derived in chapter 3.2 is applied for the experiment 3, 5, 7, and 8 to investigate the diffusion coefficient. Figures 3.5 and 3.6 shows results for the experiments respectively. The dotted lines are the overall diffusion coefficients calculated for the experiments.

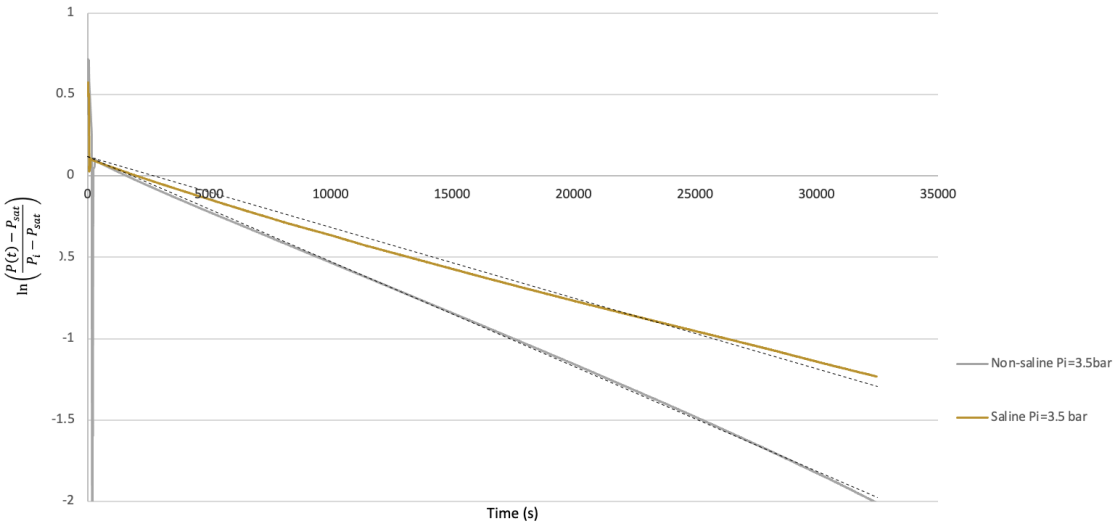

Figure 3.5: Diffusion coefficient for non-saline and saline WBS at Pi=4.50 bar

Comparing the data line giving the diffusion coefficient at each time-point to the overall diffusion coefficient trend line shows evidence of convection driven mass transfer enhancement. For all experiments the trend line intercepts the data, showing a shift from early stage convection to late stage convection. From inputting the gradient of the trendline as the $ln(\frac{P(t)-P_{sat}}{P_i-P_{sat}})$ term in equation 1.41 the diffusion coefficient was determined. Table 3.3 shows an overview of the diffusion coefficients calculated. Again, the effect of increased P_i and salt are apparent.

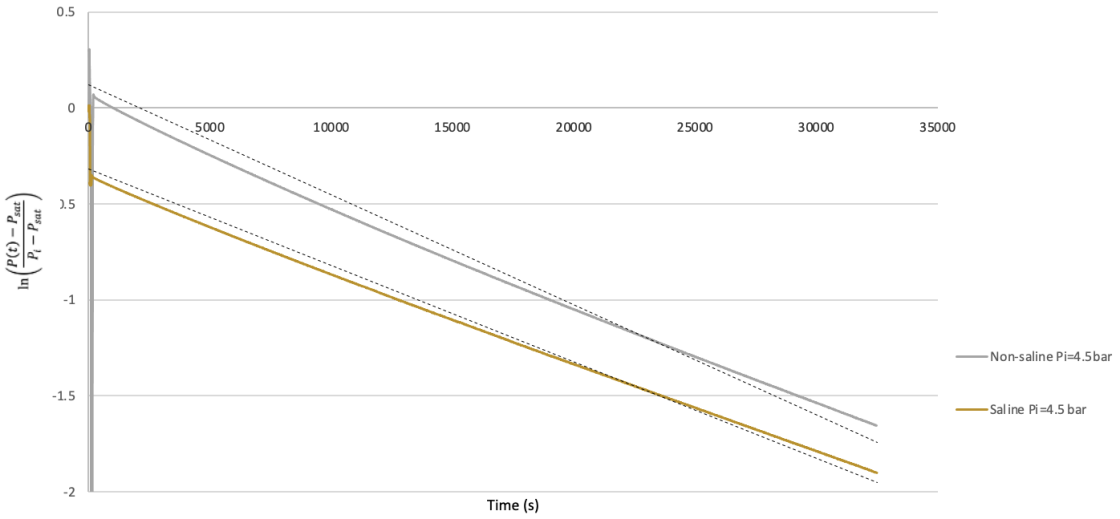

Figure 3.6: Diffusion coefficient for non-saline and saline WBS at Pi=4.50 bar

	P_i (bar)	P_{sat} (bar)	Overall diffusion coefficient (m^2/s)	Atwood number
Experiment 3	4.80	1.90	$-6 \cdot 10^-5$	0.0009
Experiment 5	3.50	1.39	$-5 \cdot 10^-5$	0.0009
Experiment 7	4.50	1.80	$-5 \cdot 10^-5$	0.0008
Experiment 8	3.30	1.40	$-4 \cdot 10^-5$	0.0008

Table 3.3: Overall diffusion coefficient calculated

3.2 Mass balance

As outlined in the analytical method, chapter , there are two methods developed to determine the concentration of the CO_2 gas in the system. Both the real gas law and a modification, Van der Waal's equation 1.44, were applied in the mass balance. Van der Waal's method only gave valid results for the first experiment. It is possible the coefficients used are not applicable at pressures investigated. Therefore the real gas law is used for further analysis.

3.2.1 Non-saline WBS

Table 3.4 shows the results from the mass transfer analysis derived in chapter 1.4.

Table 3.4: Mass balance for CO_2 in non-saline WBS.

	n_{in} ($\cdot 10^4$ mol)	n_{sat} ($*10^4$ mol)	$n_{flashed}$ ($\cdot 10^4$ mol)	Discrepancy ($\cdot 10^4$ mol)
Experiment 1	1004.84	358.39	7.37	639.08
Experiment 2	901.45	341.32	6.47	605.59
Experiment 3	780.20	317.83	6.42	455.94
Experiment 4	696.89	263.14	5.04	428.72
Experiment 5	551.52	232.56	3.82	315.57

There is a clear relationship between the initial pressure and the amount of CO_2 absorbed in total. The increase in solubility with pressure is supported by both the literature research carried out in preparation for the laboratory work as well as the pressure decay result. Quantifying the absorbed CO_2 is proof of this hypothesis. The results are displayed in figure 3.7

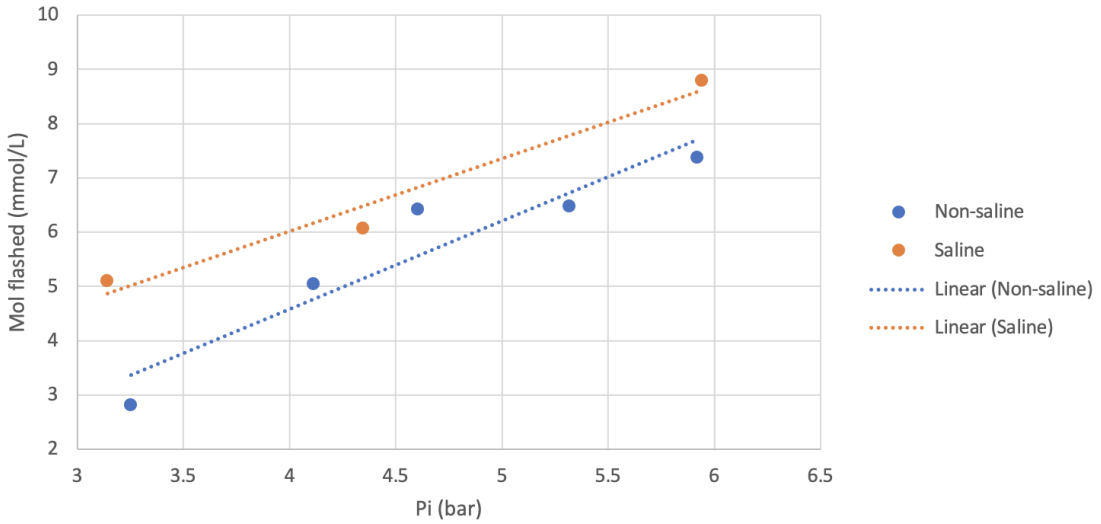

Figure 3.7: Visual evidence of enhanced mass transfer due to convection in non-saline WBS.

Another method of analysing the results is to find the percentage of mol CO_2 absorbed per mol CO_2 in the gas cap at the initial pressure. The percentage is plotted against P_i in figure 3.8. From equation 1.18 we know that the number of moles present at P_i is directly proportional to the number of moles. This figure is presented to remove the effect of the pressure to view the consistency of the results obtained. As there are many factors that are difficult to control as well as potential for significant human error due to the experiment being relative analogue, investigation into the consistency of the results was considered important. The values on the y-axis should be similar for all the pressures using non-saline and saline WBS respectively. There is some variation indicating inconsistencies as expected from the reasons outlined.
As mentioned earlier, the sample size is too small to make an accurate conclusion confidently. The discrepancies are also large and need to be evaluated further. This is discussed further in 5.

3.2.2 Saline WBS

Table 3.5 shows the results from the mass transfer analysis derived in chapter 1.4.

Table 3.5: Mass balance for CO_2 in saline WBS.

	n_{in} ($*10^4$ mol)	n_{sat} ($*10^4$ mol)	n_{fashed} ($*10^4$ mol)	Discrepancy ($*10^4$ mol)
Experiment 1	1007.38	370.03	8.79	628.85
Experiment 2	801.08	326.29	6.08	468.71
Experiment 3	579.61	254.41	5.11	320.01

In figure 3.7 the mol flashed, hence absorbed by the liquid, are presented. The trend line added shows similar trends between pressure and non-saline. It is observed the slope of the non-saline data being steeper, showing a stronger correlation between pressure and solubility compared to the saline WBS. This is expected, as previously established the solubility in general is lower for non-saline WBS. This agrees with the article published by the Chemical Geology journal evaluating the relationship between salinity and pressure and the effect this has on the solubility(24) .
From table 3.4 and 3.5 it is clear the discrepancies are significant. Some CO_2 remained in the flash cell

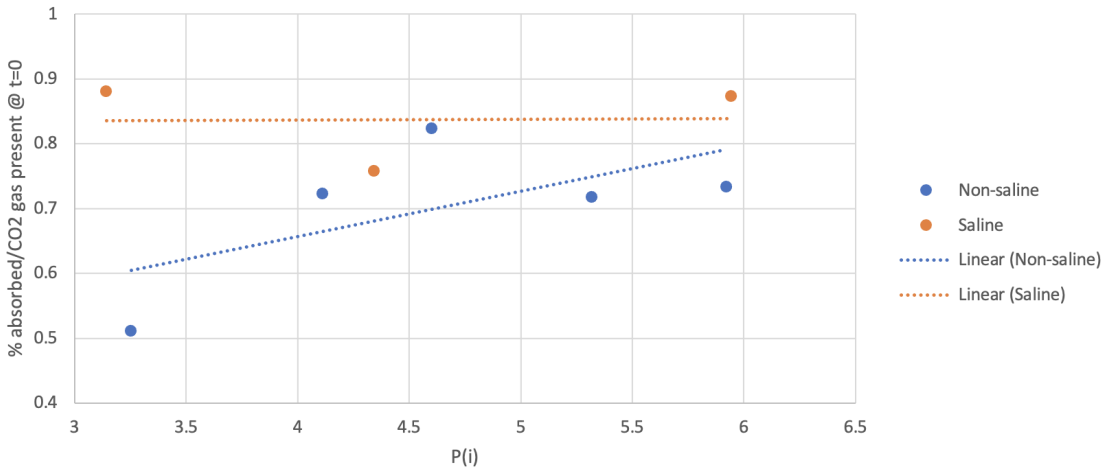

Figure 3.8: Visual evidence of enhanced mass transfer due to convection in non-saline WBS.

where the liquid accumulated and in the tubes from the flash cell to the gasometer. However, this is not of large enough magnitude to account for the discrepancies. It was observed, as displayed in figure 3.9 that shows CO_2 being desorbed after the flash distillation step once a sample had been obtained for pH and density measurements. It is also possible that there was an undetected leak due to not having pressure transmitters connected to the flash cell.

3.2.3 Remaining CO_2 after flashing

As bubbles were observed in the liquid after flashing, as seen in figure 3.9 it was carried out an analysis to determine the final concentration of the WBS. Equation 1.51 and 1.52 were employed for this purpose. The following table gives the calculated final concentration of CO_2

Table 3.6: Remaining CO_2 in the system

	$P_i(bar)$	$P_{sat}(bar)$	Remaining concentration (mol/m)
Experiment 3	4.80	358.39	$1.98 \cdot 10^{-12}$
Experiment 5	3.50	341.32	$1.75 \cdot 10^{-12}$
Experiment 7	4.50	317.83	$1.35 \cdot 10^{-12}$
Experiment 8	3.30	263.14	$2.38 \cdot 10^{-12}$

From the data we can conclude that the remaining CO_2 in the WBS is negligible. The discrepancies in the mass balance therefore remain high.

3.3 Visual observations

To enable to visually observe the saturation of the WBS a recording of each experiment was made using a smartphone and a monopod screwed to the table of the experimental apparatus. The following figures show a time lapse of experiment 1, 3 and 5 for non-saline WBS and 1 and 3 for the saline WBS. Experiment 2 and 4 for saline WBS and experiment 2 for saline WBS has been voided from being presented in the report to keep it from being too long. The specific experiments presented was chosen for maximum range of initial pressures to investigate the effect it has on the mass transfer mechanisms and rats. It took approximately 60 seconds from t=0 until 380 ml of WBS had been drained from the

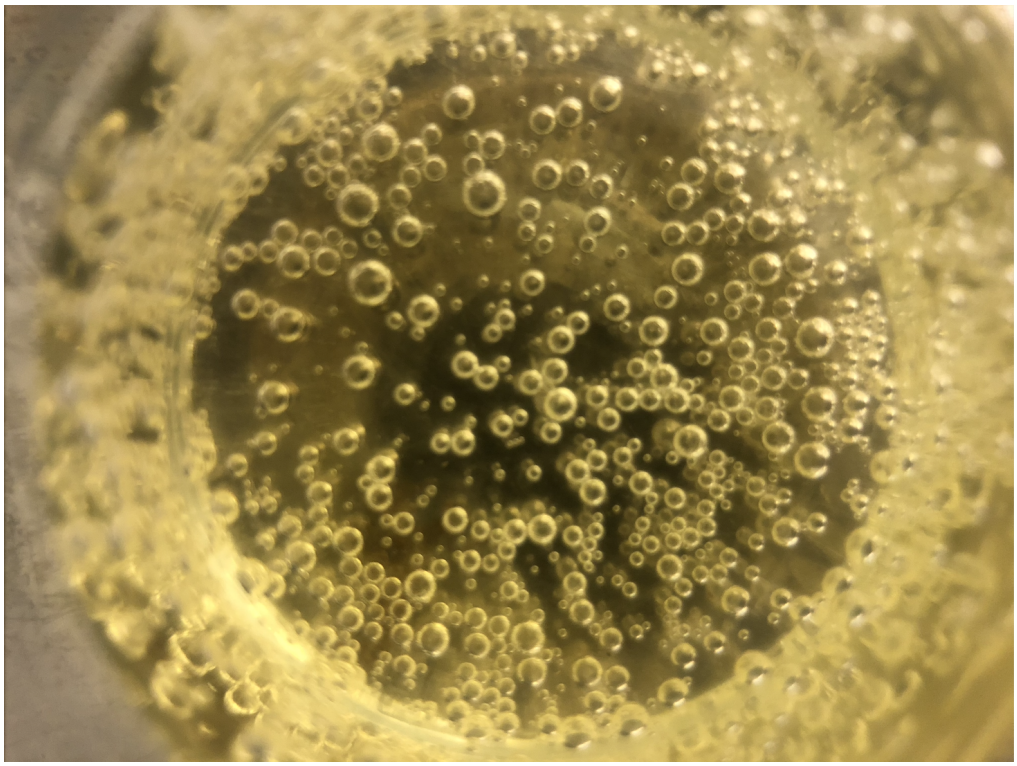

Figure 3.9: CO_2 bubbles desorbed from WBS after flashing

cell. Therefore 60 seconds is added to the first time interval for the picture. For the remaining pictures an interval of 110 seconds was used.
The picture series are presented in figure 3.12, 3.13, 3.14, 3.16, 3.17, 3.18.

Non-saline WBS

The following figures show visual evidence of convection driven diffusion in non-saline WBS.
In the pictures the pH indicator provides clear evidence that there is mixing due convection. This can also be seen in the time series, where it is observed convection occurring from the start of the experiment, t=0. The mixing patterns highlighted can be compared to figure 1.5.
From the time series displayed in figure 3.12, 3.13, 3.14 the mixing regime is turbulent due to the large density difference between the liquids. This is backed up by the Atwood equation displayed in chapter 1.4.

Saline WBS

The following figures show visual evidence of convection driven diffusion. Figure 3.11 shows evidence of convection in saline solution.
When investigating the time series it was apparent that the there was a clear divide between the saturated and non-saturated WBS. It is suspected that the salt concentration was not consistent when pumped into the cell. This explains the phenomenon which is apparent in the time series, figure 3.16, 3.17 and 3.18. From evaluating Atwood's number for the saline WBS it makes sense for convection to occur at a slower, laminar regime. However, it does not explain the phenomenon observed in the saline time series. There is a clear horizontal boundary where diffusion seemed to be at arrested development, before eventually breaking through the boundary and saturating the rest of the WBS. It is suspected

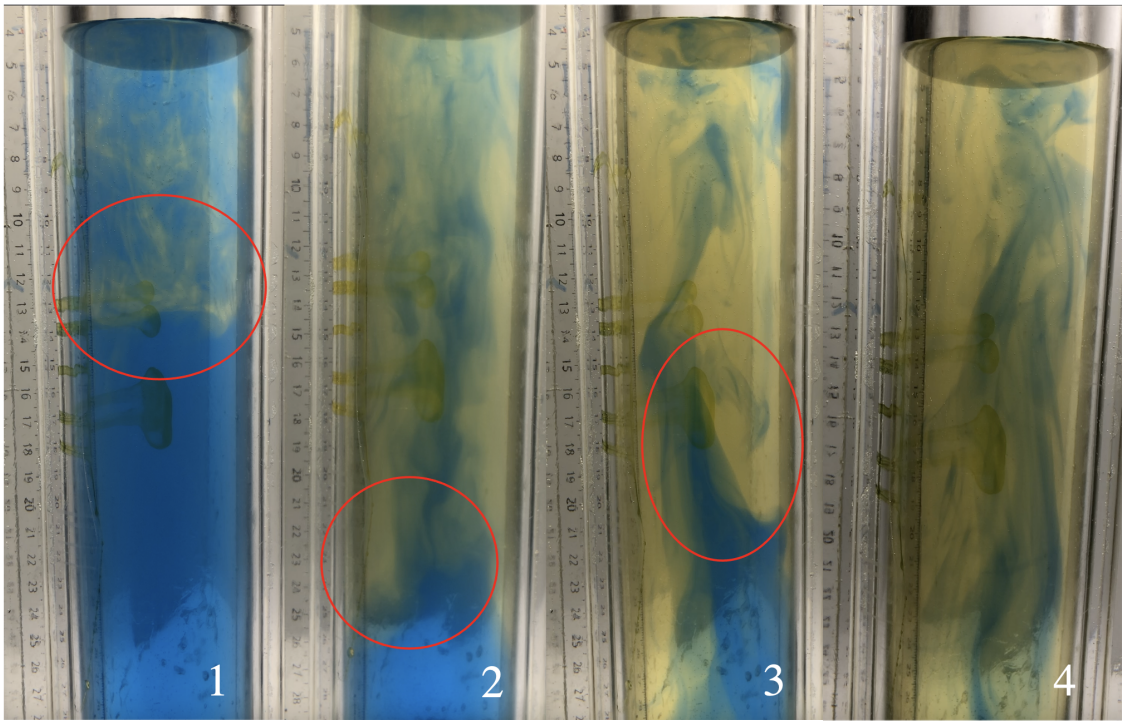

Figure 3.10: Visual evidence of enhanced mass transfer due to convection in non-saline WBS.

the salt concentration in the PVT was not consistent, hence the more concentrated solution accumulating at the bottom of the cell. This can be due to insufficient mixing before pumping the solution into the cell, resulting in a non-homogeneous solution. Simply relying on visual cues for determining the proved to be insufficient, it should have been either brought to a boil or homogenized. This would have led to a more accurate experiment.

When the recording for experiment 8 was carried out the video clip was cut short, which is why it ends before the whole L is saturated. However it showed similar trends as experiment 6 towards the end.

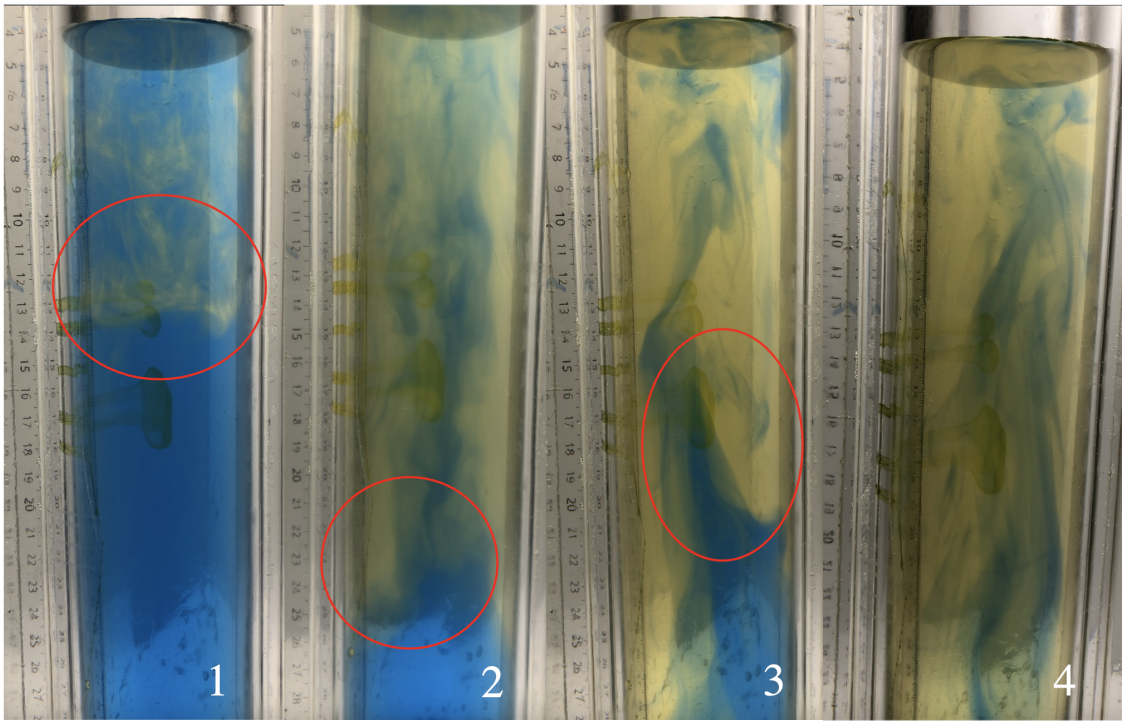

Figure 3.11: Visual evidence of enhanced mass transfer due to convection in saline WBS.

Saline solutions

Figure 3.15 displays visable convection patterns in the saline solution.
The following figures show the time series of the experiments conducted using saline WBS in the order low to high initial pressure.

3.4 Application of results to injection into aquifer

In a real CO_2 injection scenario the initial pressure of the CO_2 plume would be significantly higher than those investigated in this experimental work. The capillary entry pressure for the reservoir sand at the Utsira formation, the only saline aquifer used for CCS purposes, is 4 bar, so this makes it clear the injection pressure needs to be significantly higher for effective diffusion to take place (25) . This is due to limitations of the equipment. The PVT cell was already damaged from previous use at pressure over the specified limit at 7 bar. Though the damage was repaired through the addition of the epoxy mould, successfully sealing the crack, it was important to be cautious of the pressures the cell was exposed to. It was decided that it was more important to focus on the mass transfer mechanisms, opposed to trying to replicate a real operation. Having a clear visual picture was considered a priority to observe the effect of convection in particular. Therefore the clear PVT cell with pressure limitations was favoured over a steel PVT cell.

Despite not representing a real scenario the thesis provides valuable research on the flow mechanisms occurring at early and late stage diffusion .

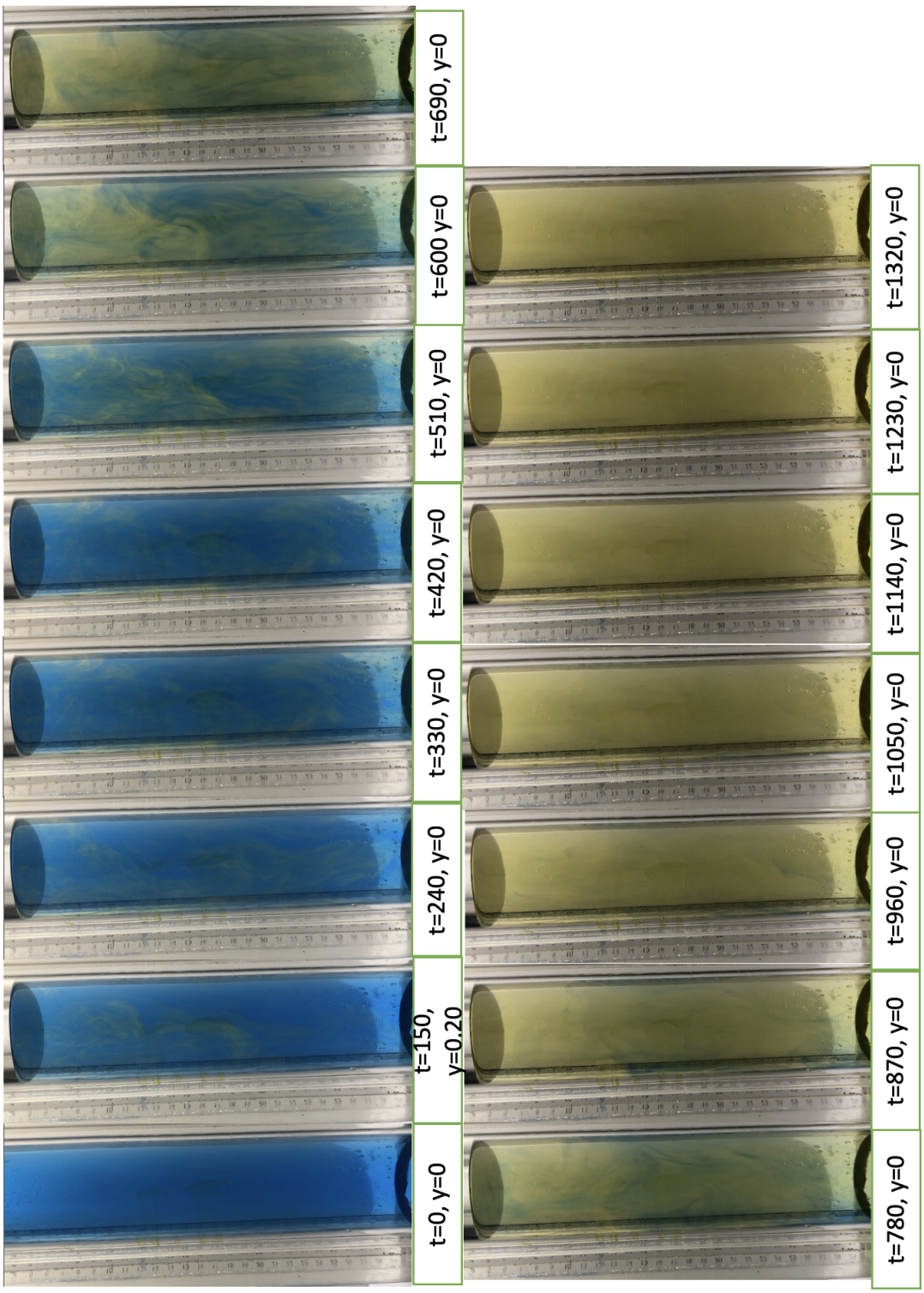

Figure 3.12: Time series of mixing regime by convection in non-saline WBS with $P_0 = 3.50bar$

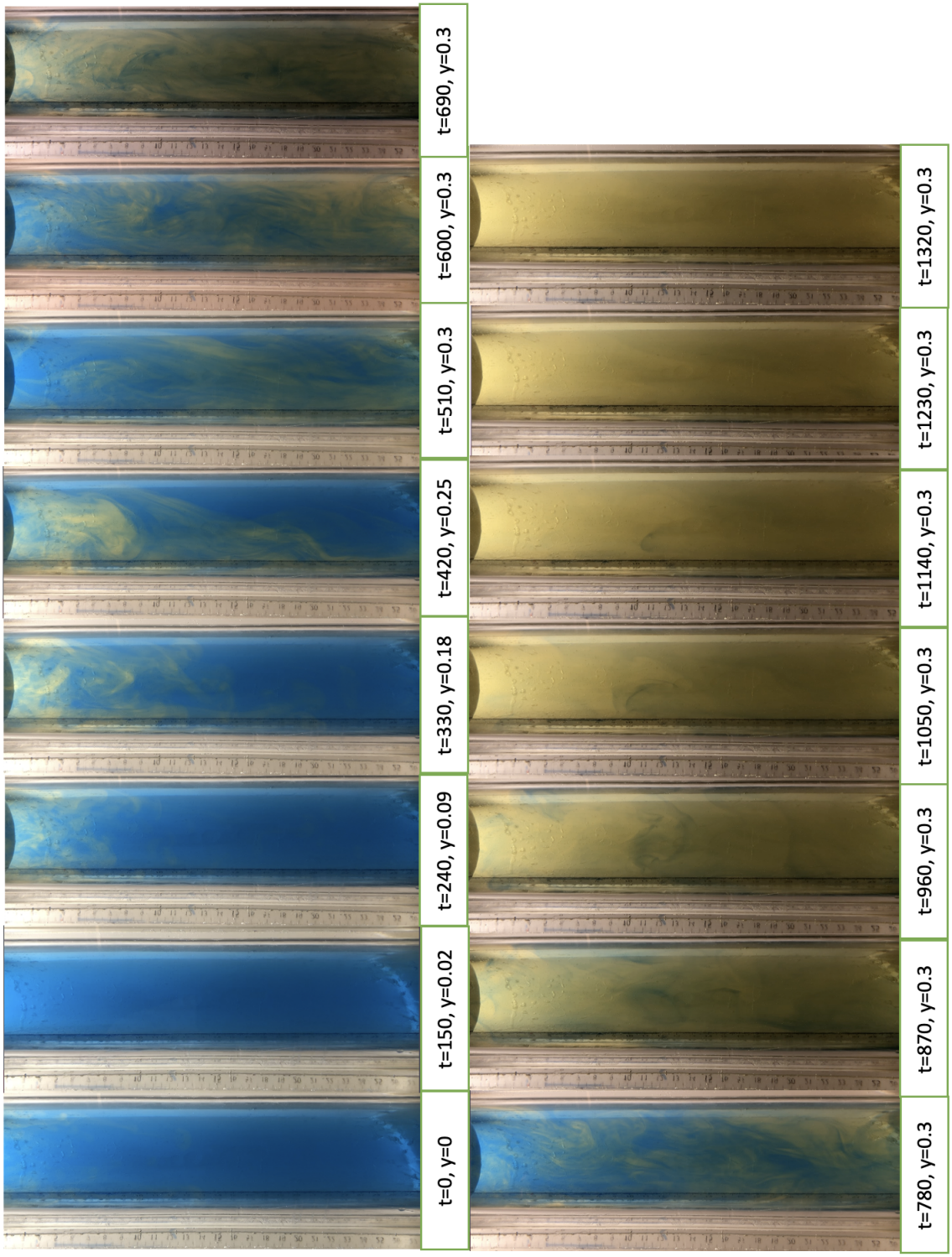

Figure 3.13: Time series of mixing regime by convection in non-saline WBS with $P_i = 4.80bar$

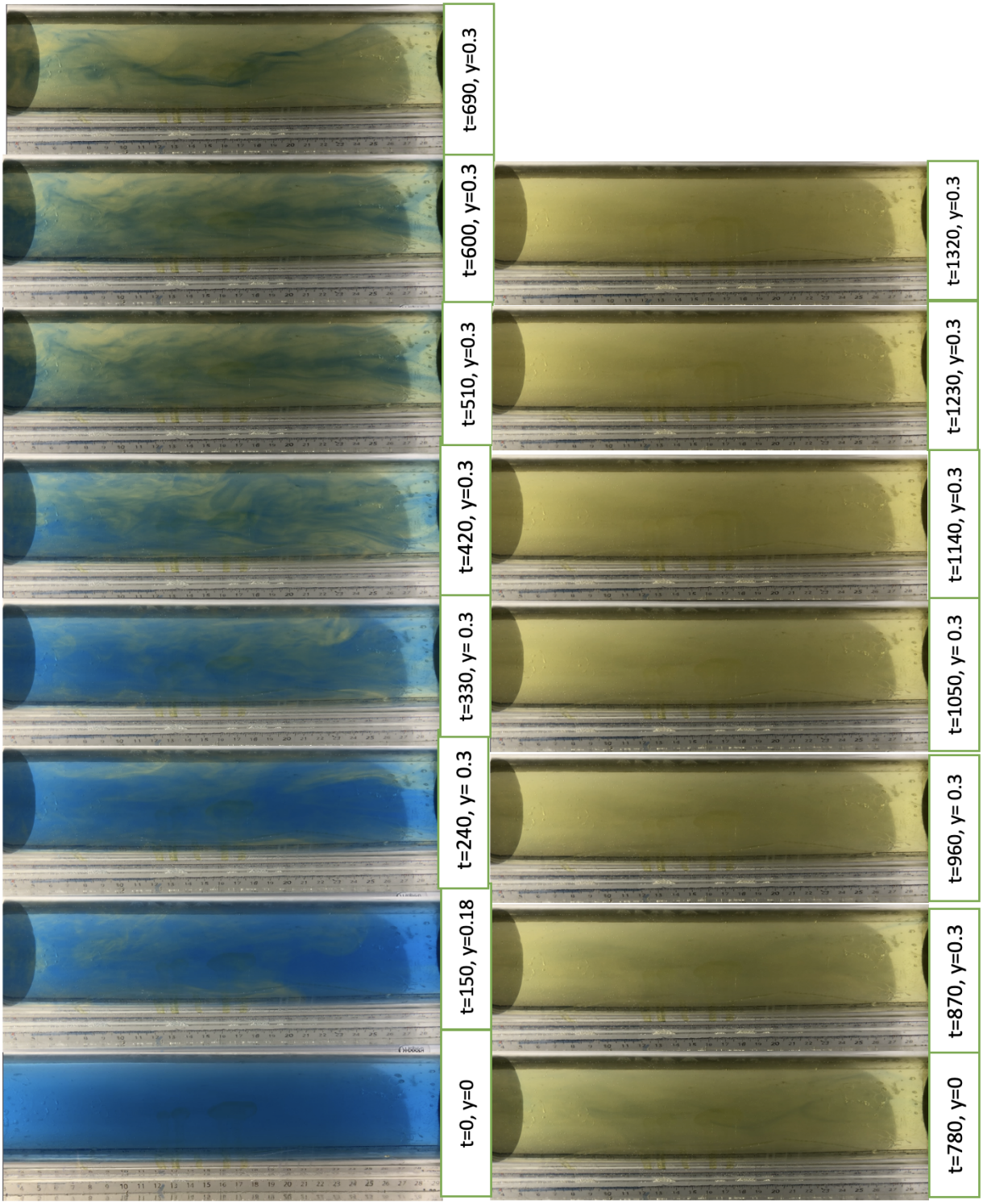

Figure 3.14: Time series of mixing regime by convection in non-saline WBS with $P_i = 6.10bar$

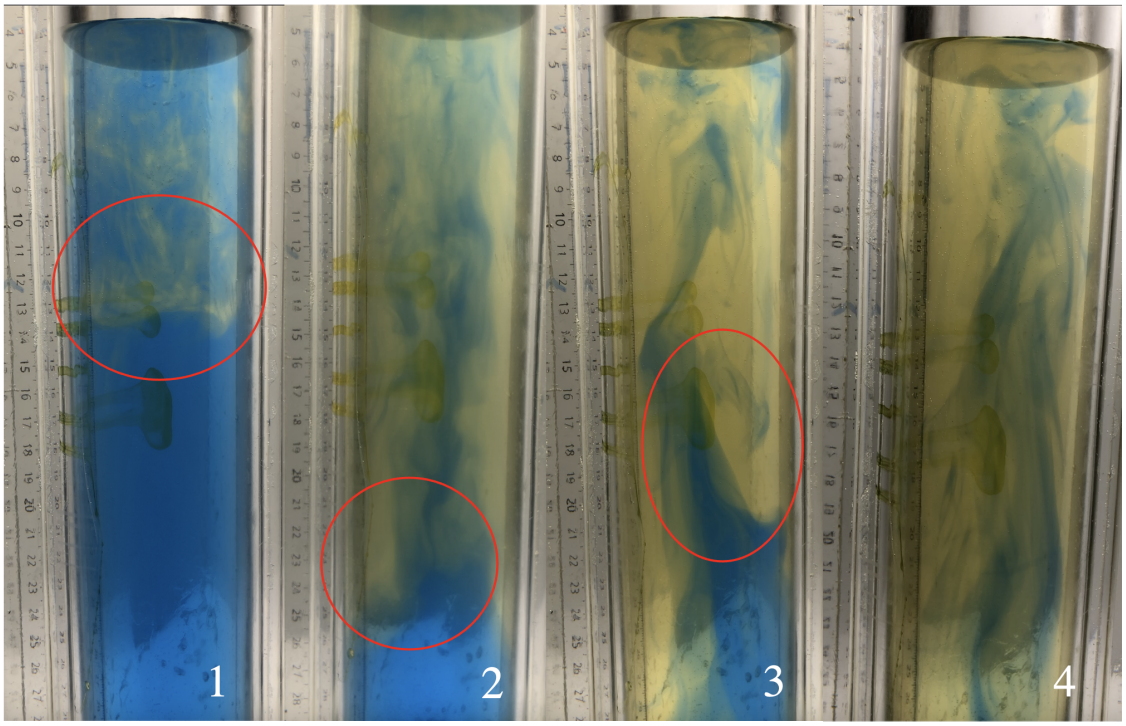

Figure 3.15: Visual evidence of enhanced mass transfer due to convection in saline WBS.

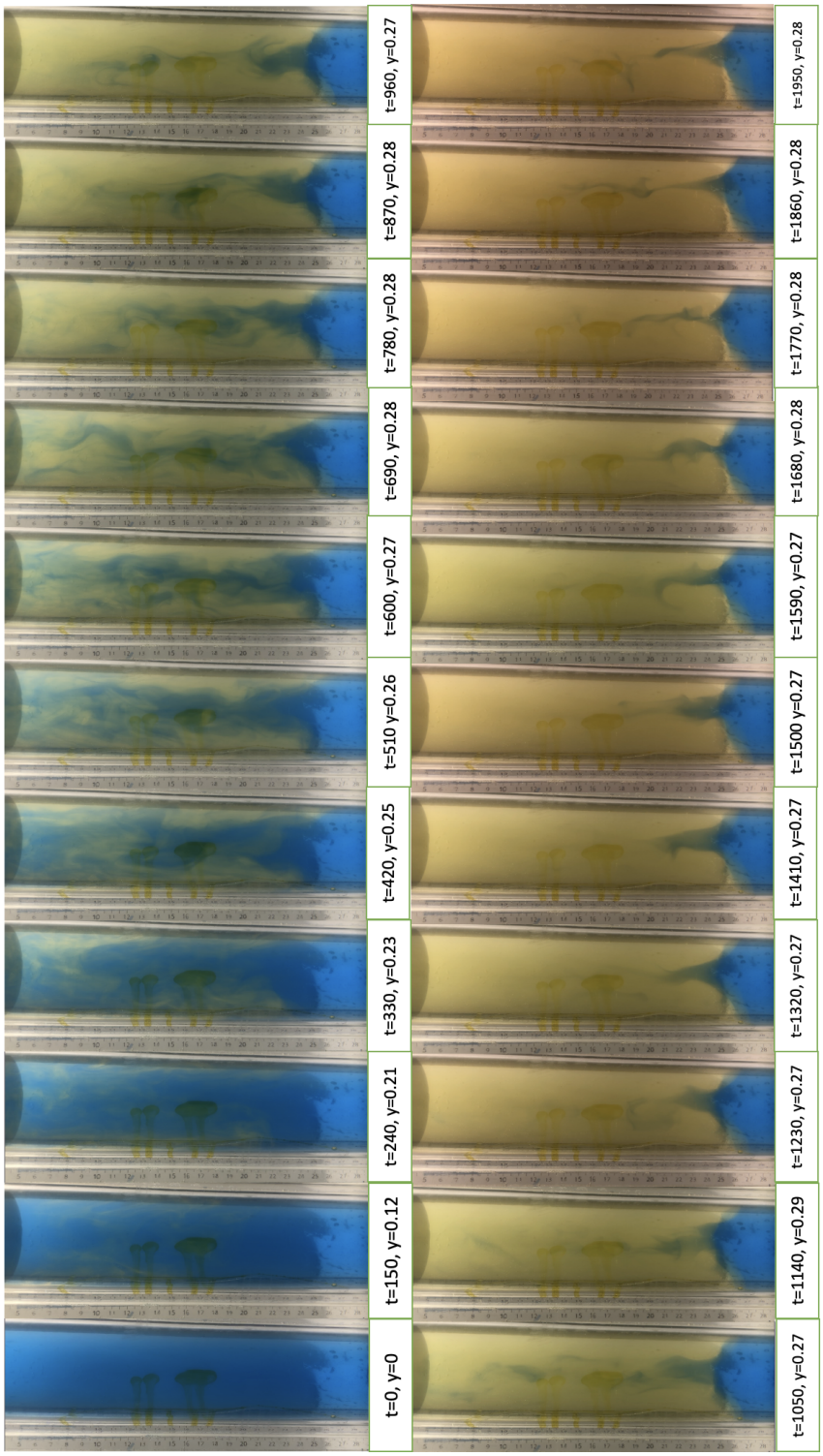

Figure 3.16: Time series of mixing regime by convection in saline WBS with $P_i = 6.10bar$

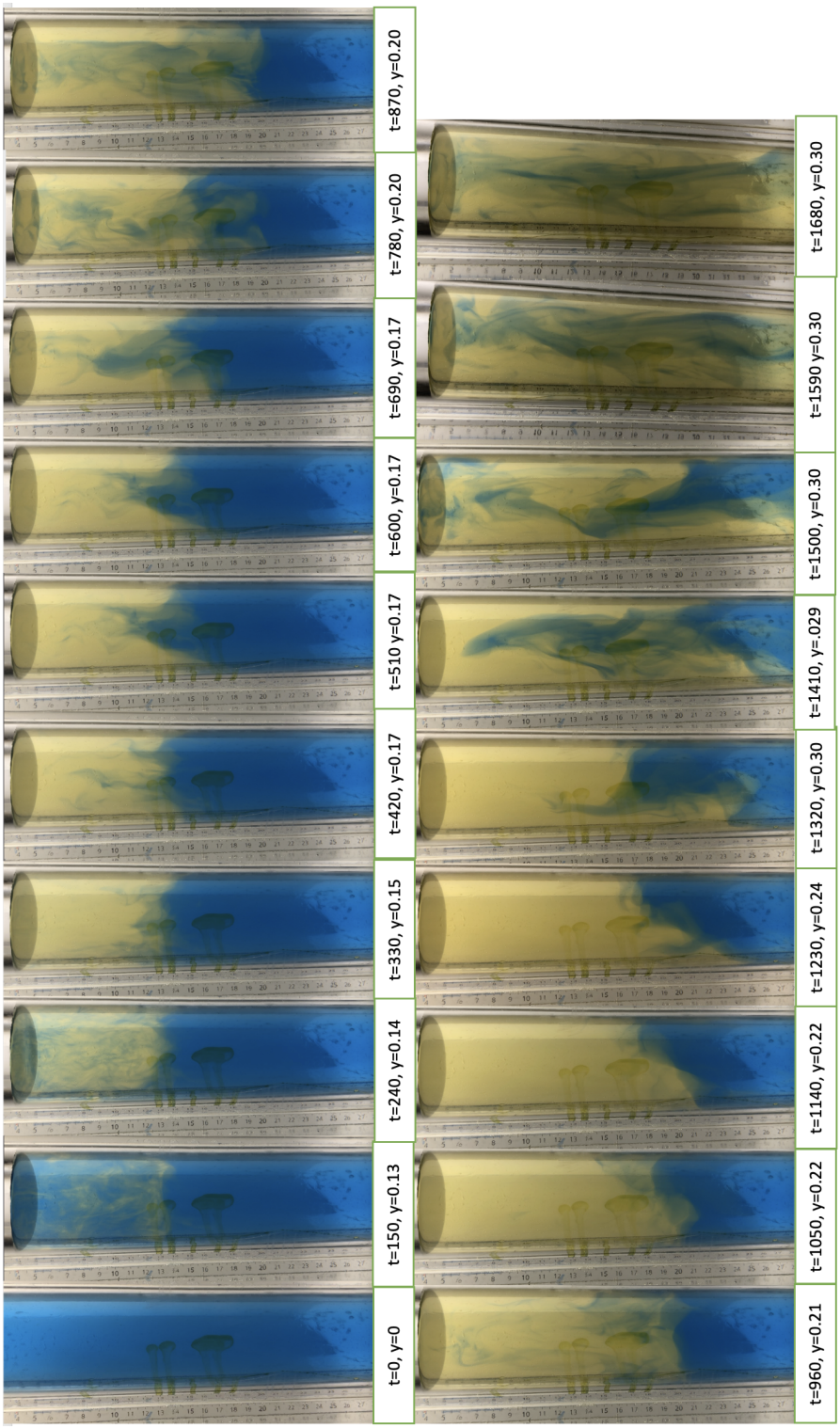

Figure 3.17: Time series of mixing regime by convection in saline WBS with $P_i = 3.50bar$ (P1/2)

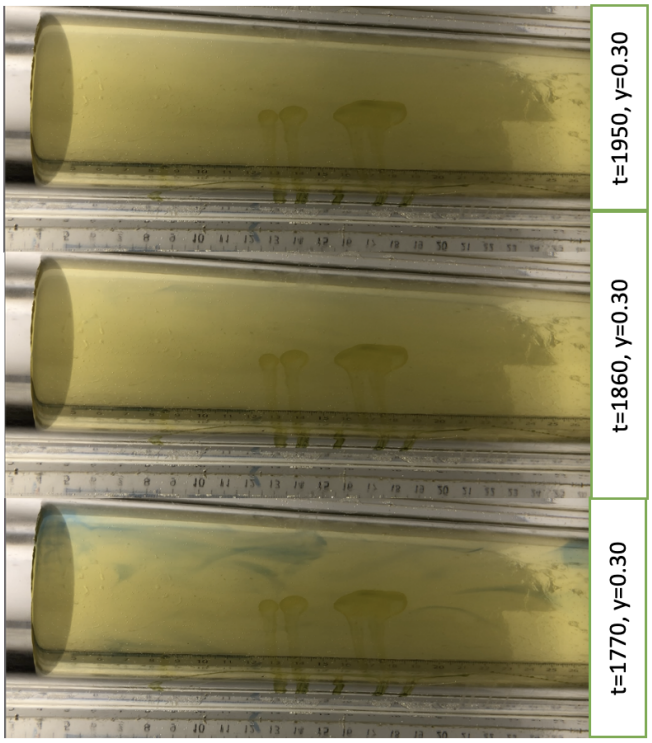

Figure 3.18: Time series of mixing regime by convection in saline WBS with $P_i = 4.80bar$ (P2/2)

Chapter 4

Conclusion

The work carried out was to further research on injection of CO_2 for permanent storage in deep aquifers. The experimental work consisted of investigating the absorption mechanisms inside a transparent PVT cell cast in an epoxy resin block. A flash distillation cell was then used for a mass balance of the CO_2 to be carried out. A simple pressure decay model was derived to study the diffusion rate. Although invalid P_{sat} were calculated for the experiments run at low pressures it still gave a fairly accurate model which allowed the diffusion coefficient to be investigated.
The results obtained for the pressure decay showed clear definition of having several stages of diffusion as the trend curve fitted to the natural log pressure curve, which was used to determine the diffusion coefficient, intersected the curve, showing a shift in diffusion rates. Acceleration in the diffusion was through the visual analysis confirmed to be due to instabilities in the solution due to increased gravity at the gas-liquid interface. This was clear from visible fingers dropping in a vertical direction, followed by diffusion in horizontal direction. Mixing decelerates as the solution approaches full saturation which is important when linking the results to storage as this could have an effect on the structural foundation of the formation.
A comparison of the results obtained for the saline and non-saline WBS gave insight into the effect of increased ionic strength.
As addressed in the results, homogenization of the brine has proved to be important as there was clear inconsistencies in the concentration in the PVT cell. This is evident from both time series for the saline solution where there diffusion comes to a temporary stop at a length y, before eventually saturating the rest of the cell. Simply shaking the flask until there was no visible salt in the solution proved not sufficient. Despite this compromising the results, it is only expected to effect the diffusion rate, not the overall absorption of the system. Conclusions can therefore still be made on the effect the increased saturation of ions in the solution.
As expected the addition of NaOH in the solution inhibited absorption of CO_2 which was highlighted by the lowered diffusion coefficient compared to the results obtained using the non-saline WBS at the same P_i. This is important to consider when evaluating a potential aquifier formation for permanent storage as an increase in salinity highly reduces the diffusion rate and overall absorption CO_2 leading to decreased storage capacity.
A flash distillation cell and was incorporated to quantify the gas absorbed by the WBS. This allowed for a mass balance to be carried out. Despite the discrepancy being large between the moles in and moles out, the method gave consistent results compared to literature, where a clear link between

pressure and solubility was established. This indicates that high injection pressures are favoured, however the pressure limitations of the formation and the cap rock need to be carefully considered.

Chapter 5

Further work

An experiment cycle takes at least 24 hours depending on the initial pressure. It is a time and work intensive process consisting of pressure tests, flushing of the cell. Therefore the final experimental data set was somewhat smaller than anticipated. Obtaining three sets of experimental data per pressure point chosen would give more insight into the consistency of the results. Although clear trends were observed from the data obtained.
To build on this point it would be valuable to be able to determine the local concentrations in the cell. This could be done using the pH but would potentially be difficult to do accurately due to the human error associated with comparing the colors to the reference chart. Carrying out the experiment with porous packing would give a more accurate representation of the , however the pressure in the cell might lead to unstable packing. Adding polymers is also an area of interest as it would be possible to relate the results to the absorption/desorption process for the capture part of the CCS cycle.

References

[1] A. Olhoff, J. Partnership, T. Kuramochi, J. Rogelj, N. Höhne, K. Jiang, and T. Fransen, "Emissions gap report 2019," 11 2019.

[2] B. Praetorius and C. Von Stechow, "Electricity gap versus climate change: electricity politics and the potential role of ccs in germany," *Meadowcroft, James/Langhelle, Oluf: Caching the Carbon. The Politics and Policy of Carbon Capture and Storage, Cheltenham/Northampton*, pp. 125–157, 2009.

[3] A. Tjernshaugen and O. Langhelle, "Technology as political glue: Ccs in norway," *Meadowcroft, James/Langhelle, Oluf: Caching the Carbon. The Politics and Policy of Carbon Capture and Storage, Cheltenham/Northampton*, pp. 98–124, 2009.

[4] A. Swanger, "The power of the universe:'what we can learn from nasa on hydrogen'," in *Webinar—The power of the Universe:'What we can learn from NASA on Hydrogen'*.

[5] L. I. Helgesen, G. Cauchois, T. Nissen-Lie, M. Prestholdt, M. Carpenter, and A. Røsjorde, "co_2 footprint of the norwegian longship project," *Available at SSRN 3821398*, 2021.

[6] G. E. IEA, "Co2 status report 2021," *International Energy Agency, Paris*, vol. 562, 2021.

[7] V. P. Oktyabrskiy, "A new opinion of the greenhouse effect," *St. Petersburg Polytechnical University Journal: Physics and Mathematics*, vol. 2, no. 2, pp. 124–126, 2016.

[8] A. Olabi, K. Obaideen, K. Elsaid, T. Wilberforce, E. T. Sayed, H. M. Maghrabie, and M. A. Abdelkareem, "Assessment of the pre-combustion carbon capture contribution into sustainable development goals sdgs using novel indicators," *Renewable and Sustainable Energy Reviews*, vol. 153, p. 111710, 2022. [Online]. Available: https://www.sciencedirect.com/science/article/pii/S1364032121009849

[9] S. T. Munkejord, M. Hammer, and S. W. Løvseth, "Co2 transport: Data and models – a review," *Applied Energy*, vol. 169, pp. 499–523, 2016. [Online]. Available: https://www.sciencedirect.com/science/article/pii/S0306261916300885

[10] K. Bjørlykke, "Introduction to petroleum geology," in *Petroleum Geoscience*. Springer, 2015, pp. 1–29.

[11] M. R. Riazi, "A new method for experimental measurement of diffusion coefficients in reservoir fluids," *Journal of Petroleum Science and Engineering*, vol. 14, no. 3-4, pp. 235–250, 1996.

[12] S. Zarghami, F. Boukadi, and Y. Al-Wahaibi, "Diffusion of carbon dioxide in formation water as a result of co_2 enhanced oil recovery and co_2 sequestration," *Journal of Petroleum Exploration and Production Technology*, vol. 7, no. 1, pp. 161–168, 2017.

[13] R. Farajzadeh, "Enhanced transport phenomena in co_2 sequestration and co_2 eor," 2009.

[14] T. M. Tungesvik, Rabenjafimanantsoa, "Visualization of co_2 absorption in newtonian and non-newtonian fluids," 2012.

[15] T. Hansen, "An experimental study of the enhanced mass transfer process by co_2 absorption for carbon storage in saline aquifers," 2020.

[16] Y.-J. Lin, E. Chen, and G. T. Rochelle, "Pilot plant test of the advanced flash stripper for co_2 capture," *Faraday discussions*, vol. 192, pp. 37–58, 2016.

[17] C. o. E. The University of Utah, "Lecture 4: Diffusion, flicks 1st equation," no. 1-3, https://my.eng.utah.edu/ lzang/images/lecture-4.pdf.

[18] D. L. Youngs, "Numerical simulation of turbulent mixing by rayleigh-taylor instability," *Physica D: Nonlinear Phenomena*, vol. 12, no. 1-3, pp. 32–44, 1984.

[19] O. Izgec, B. Demiral, H. Bertin, and S. Akin, "co_2 injection into saline carbonate aquifer formations i," *Transport in porous media*, vol. 72, no. 1, pp. 1–24, 2008.

[20] K. Peterson and W. Klemperer, "Structure and internal rotation of h2o–co2, hdo–co2, and d2o–co2 van der waals complexes," *The Journal of chemical physics*, vol. 80, no. 6, pp. 2439–2445, 1984.

[21] Y. A. Cengel, *Fundamentals of thermal-fluid sciences*, ser. McGraw-Hill higher education. McGraw-Hill, 2012.

[22] K. Peterson and W. Klemperer, "Structure and internal rotation of h_2o--co_2, $hdo--co_2$, and $d2o--co_2$ van der waals complexes," *The Journal of chemical physics*, vol. 80, no. 6, pp. 2439–2445, 1984.

[23] J. E. Garcia, "Density of aqueous solutions of co2." [Online]. Available: https://www.osti.gov/biblio/790022

[24] S. Portier and C. Rochelle, "Modelling co_2 solubility in pure water and *nacl*-type waters from 0 to 300 c and from 1 to 300 bar: Application to the utsira formation at sleipner," *Chemical Geology*, vol. 217, no. 3-4, pp. 187–199, 2005.

[25] R. Chadwick, G. Williams, J. Williams, and D. Noy, "Measuring pressure performance of a large saline aquifer during industrial-scale co_2 injection: The utsira sand, norwegian north sea," *International Journal of Greenhouse Gas Control*, vol. 10, pp. 374–388, 2012.

Chapter 6

Appendix

6.1 Appendix A: Fourier series derivation

To determine a term for a_n the following derivation is carried out.
Fick's second law, displayed in figure 1.7, predicts the concentration of a gas diffusing into a solution column as a function of column height and time. When applying Fourier analysis the variables are evaluated separately. This will provide infinitely many solutions of equation 1.7 at the predefined boundaries. This results in the following equation.

$$c(t,y) = a_m exp(\frac{-t}{\tau_m}) sin(\kappa_m y) \tag{6.1}$$

As Fick's second law is linear the general solution to equation 6.1 is the sum of the solutions given from $n = 0 - \infty$, also known as the superposition.

$$c(t,y) = a_0 + \sum_{n=0} a_n exp(\frac{-tD(2n+1)^2\pi^2}{4L^2}) sin(\frac{(2n+1)\pi y}{2L}) \tag{6.2}$$

a_n is calculated from the initial data at y=0, shown in equation 6.3. a_n is calculated by the gas concentration in the liquid column at t=0, shown in equation 6.4.

$$c(t, y=0) = a_0 = c_{sat} \tag{6.3}$$

$$c(t,y) = a_0 + \sum_{n=0}^{inf} a_n sin(\frac{(2n+1)\pi y}{2L} \tag{6.4}$$

Both sides of the above term, 6.4 is multiplied by the sin mode displayed in 6.5 and integrated over the domain 0¡y¡L resulting in equation 6.6

$$sin((\frac{(2m+1)\pi y}{2L} \tag{6.5}$$

$$\begin{aligned} \int_0^L c(t=0,y) sin(\frac{(2m+1)\pi}{2L} dy = a_0 \int_0^L (\frac{(2m+1)\pi}{2L}) dy \\ + \sum_{n=0} a_n [sin(\frac{(2n+1)\pi y}{2L}) sin \frac{(2n+1)\pi y}{2L} dy] \end{aligned} \tag{6.6}$$

LHS becomes zero as there is no present gas at t=0. The results are only valid when m=n:

$$0 = a_0 \int_0^L sin(\frac{(2n+1)\pi y}{2L})dy + \sum_n^\infty = 0a_n[\int_0^L sin^2(\frac{(2n+1)\pi y}{2L})dy] \tag{6.7}$$

resulting in the following equation

$$0 = a_0(\frac{-2L}{(2n+1)}\pi[cos(\frac{(2n+1)\pi y}{2L})]_0^L) + \sum_{n=0} \frac{a_n}{2}(y - \frac{L}{(2n+1)\pi}[sin(\frac{(2n+1)\pi y}{L}]_0^L) \tag{6.8}$$

$$a_n = -a_0 \frac{4}{(2n+1)\pi} \tag{6.9}$$

6.2 Appendix B: Temperature calibration

To ensure the values for temperature obtained through the Pasco absolute temperature and pressure transmitter setup were accurate the following calibration was carried out.
The Fluke dry well calibration tool was utilised for this purpose. The equipment allows for different temperature set points to be programmed in advance. The temperature range 0-40 $°C$ was used with an interval of 5 $°C$. It was ensured the temperature of the fluke dry well remained stable for at least a minute before the temperature pair was recorded from both the computer obtained value through Pasco and from the Fluke dry well display.
The method outlined gave a set of 9 data pairs which is considered an adequate sample size. The values obtained from both temperature sensors are displayed below in table 6.1

PASCO ($°C$)	Fluke dry well ($°C$)
0.90	1.13
5.10	5.33
10.10	10.36
15.10	15.32
20.00	20.27
25.10	25.25
30.00	30.22
35.10	35.23
40.00	40.20

Table 6.1: Temperature values obtained from Pasco temperature sensor and the Fluke dry well.

The values were plotted against each other to show the data pairs graphically in a chart as shown below in figure 6.1 Adding a trend line and obtaining the equation for said trend line will give the equation for calibration of the temperature.

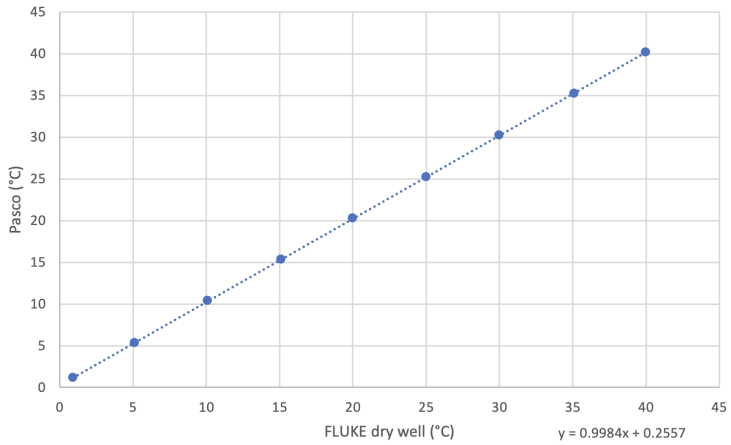

Figure 6.1: Temperature calibration plot

Solving the equation given by the trend line for X will give the true calibrated temperature value converted from the Pasco transmitter values. It is clear the the calibration result indicates properly working equipment due to the consistency of the data points. They are all placed directly on the trend line giving an R-value of 0.992.

6.3 Appendix C: Pressure calibration

To ensure the values for temperature obtained through the Pasco absolute temperature and pressure transmitter setup were accurate the following calibration was carried out.
The values obtained from the Pasco transmitter was compared to values obtained through calculations. Equation 6.10 was employed for this purpose.

$$P = \rho g h \tag{6.10}$$

Table 6.2: Pressure values obtained through calculation and Pasco pressure sensor.

$\rho g z$ $(mbarC)$	Pasco $(mbarC)$
1294.62	1297.21
1220.32	1224.21
1199.80	1201.28
1173.65	1176.31
1159.51	1163.12
1140.86	1142.95

The values were plotted against each other to show the data pairs graphically in a chart as shown below in figure 6.2 Adding a trend line and obtaining the equation for said trend line will give the equation for calibration of the temperature.

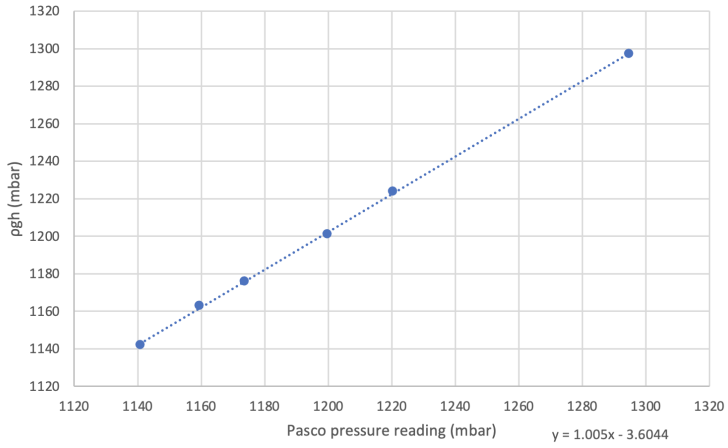

Figure 6.2: Pressure calibration plot

Solving the equation given by the trend line for X will give the true calibrated pressure values converted from the Pasco transmitter values. It is clear the the calibration result indicates properly working equipment due to the consistency of the data points. They are all placed directly on the trend line giving an R-value of 0.997.

6.4 Appendix D: Experimental procedure

Checklist for the experimental procedure

Preparation of WBS

1. A 5 l conical flask is filled with deionised water.
2. 8 doses of NaOH is added to the conical flask from a pipette set to 0.5 ml.
3. A 50 ml measuring cylinder is used to measure 37.5 ml of BTB pH indicator which is added to the conical flask.
4. If preparing a saline WBS 193.5 g of NaCl is added.
5. Mix the solution well so that it is homogeneous
6. Measure the pH level and density of the liquid using the method outlined in appendix D and E

Measuring pH of WBS

1. Turn on pH meter by pressing exit. If its already on, proceed to step 2
2. Remove electrode from storage solution and place it over the waste beaker and rinse with deionized water
3. Place the electrode in the WBS and stir gently.
4. Place the electrode on the stand so that half of the electrode submerged in the WBS.
5. Press read and wait until the pH reading stabilises before noting the value. If it does not stabalise for several minutes press read again.
6. Remove the electrode from the stand and place over the waste beaker while rinsing with deionized water.
7. Place the electrode on the stand and storage solution again.

Preparation of PVT cell

1. If the cell has been disassembled since last use, or an experiment has run with an apparent leak, a pressure-test is carried out. If the cell has not been opened since the last run, skip till step 9.
2.Connect compressed air to the top three-way valve at the outlet where the compressed CO_2 would otherwise be connected.
3. Apply grease to the threading and screw the bottom and top of the cell back on.
4. Ensure all valves are closed and all connections are tightened with a wrench.
5. The PASCO software is prepared and starts recording data. 6. The pressure on the compressed air is set to 5 bar and the top valve is opened to let the air into the cell.
7.Once the cell has a pressure of 5 bar the valve is closed. 8. Let the experiment run for a few hours.

9. The PASCO software stops recording and the data can be analysed. If the pressure has decreased significantly, more than one bar, there is a leak present in the setup. If the pressure has remained stable, move to step 12.
10. Put diswashing soap around all connections and joints where leakage can be suspected and repeat step 3-9.
11. The area surrounding the leak will visibly bubble.
12. Eliminate the leak by applying more grease or tightening the connection. If the pressure stabilises, continue to the next procedure. If not, repeat step 3-11.

Rinsing the PVT cell

Rinse the PVT cell twice by flushing it by connecting the pump to the bottom of the cell and a 5 L conical flask containing deionised water.
1. It is ensured all valves associated with the top of the cell are open so that air can be pushed out of the column to avoid pressure build-up in the cell that could damage the equipment.
2. The pump setting is first set to 50 ml/min, if it runs without issues it is switched to prime mode which is the fastest flow rate for the pump.
3. Once the cell is filled with water the pump is stopped and disconnected from the three-way valve under the cell and the cell is drained.
4. Step 2-3 are repeated once more.

Filling the cell with WBS

1. It is ensured all valves associated with the top of the cell are open so that air can be pushed out of the column to avoid pressure build-up in the cell that could damage the equipment.
2. The pump setting is set to 50 ml/min. The flowrate is kept this low to avoid air bubbles to form along the cell walls.
3. Once the liquid has reached the top of the valve connected to the CO2 tube the valve is closed.
4. The pump is immediately stopped and disconnected from the three-way valve. It is ensured the valve connected to the cell is closed to avoid leakage.

Starting the pressure decay experiment

1. The tube previously connected to the pump is placed in a measuring beaker to prepare for injection of gas and drainage of WBS once the experiment commences.
2. The LED light placed above the cell is switched on and the downlights in the rest of the laboratory are turned off
3. The smartphone is placed in the mono-pod and is adjusted so the visibility through the camera is satisfactory for interpretation.

4. The CO2 gas tank is opened and set to the specified pressure.
5. The phone is set to focus on the cell and starts recording.
6. The valve at the top of the cell is opened gently. This is done to ensure there is no air, O2 and N2, in the tubing. If air is present in the CO2 gas tube it be in the PVT cell with the gas and WBS, hence interfering with the results.
7. Simultaneously the valve at the bottom of the cell is opened to allow for drainage into the measuring beaker
8. Once the beaker shows approximately 400 ml the valve at the bottom of the cell is closed.
9. The valve at the top of the cell is left open to allow for pressure readings throughout the pressure decay run-time.
10. Once the solution inside the cell has turned yellow with no sign of blue the phone stops recording.
11. The experiments keeps until the pressure has stabilised and saturation pressure is reached.

Preparing for flashing

1. The valve on the burette is opened and a suction balloon is used to set the value to 0 ml before the valve is closed again.
2. Ensure the cup for the flash liquid is placed in the cell
3. Ensure the top of the flash cell is properly screwed on so that no thread is showing

Flashing CO_2 from P_{sat} to P_{atm}

1. Switch the three-way valve at the bottom of the cell so that the liquid drained from the cell travels into the flash cell.
2. The liquid level is insider the flash cell and the gas volume in the burette is simultaneously monitored. Once the liquid almost fills the cup the valve at the inlet of the flash cell is closed.
3. The cup containing the liquid being flashed is weighed and noted.
4. The gas volume inside the burette is noted.

6.5 Appendix E: pH measurements

A METTLER TOLEDO SevenCompact pH meter was used to measure the pH level of the WBS before and after each experiment. Table 6.3 shows the pH values associated with the experiments.

Experiment #	**Solution**	**Pre-experiment reading (pH)**	**Post-experiment reading (pH)**
Exp. 1	Non-saline WBS	10.01	5.23
Exp. 2	Non-saline WBS	9.54	5.13
Exp. 3	Non-saline WBS	9.54	5.08
Exp. 4	Non-saline WBS	9.54	5.21
Exp. 5	Non-saline WBS	10.01	5.26
Exp. 6	Saline WBS	10.01	5.04
Exp. 7	Saline WBS	10.01	5.13
Exp. 8	Saline WBS	10.01	5.42

Table 6.3: pH values for non-saline and saline WBS before and after experimental run.

6.6 Appendix F: Density measurements

Table 6.4: Densities for non-saline and saline WBS before and after experimental run.

Experiment #	**Solution**	**Pre-experiment reading (g/ml)**	**Post-experiment reading (g/ml)**
Exp. 1	Non-saline WBS	0.999	0.997
Exp. 2	Non-saline WBS	0.999	0.998
Exp. 3	Non-saline WBS	0.999	0.997
Exp. 4	Non-saline WBS	0.999	0.997
Exp. 5	Non-saline WBS	0.999	0.997
Exp. 6	Saline WBS	1.025	1.024
Exp. 7	Saline WBS	1.025	1.024
Exp. 8	Saline WBS	1.025	1.024

6.7 Appendix G: Scale up factors for flash samples

To scale up the volume of the flash samples to the volume of the WBS in the PVT cell the following scale up factors are calculated

Experiment #	**Scale up factor**
Exp. 1	178.88
Exp. 2	170.71
Exp. 3	130.69
Exp. 4	139.11
Exp. 5	217.07
Exp. 6	109.83
Exp. 7	148.37
Exp. 8	152.79

Table 6.5: Scale up factors to support mass balance calculations.